Simulation of Bulk and Grain Boundary Diffusion in B2 NiAl

Benjamin J. Soulé de Bas

Thesis submitted to the faculty of the
Virginia Polytechnic Institute and State University
In partial fulfillment of the requirement for the degree of

Master of Science
in
Materials Science and Engineering

Dr. Diana Farkas, Chairperson
Dr. Sean Corcoran
Dr. William Reynolds

May 24, 2001
Blacksburg, Virginia

Simulation of Bulk and Grain Boundary Diffusion in B2 NiAl

Benjamin J. Soulé de Bas

(ABSTRACT)

Molecular dynamics simulations of the diffusion process in ordered B2 compounds at high temperature were performed using an embedded atom interatomic potential developed to fit NiAl properties. Diffusion in the bulk occurs through a variety of cyclic mechanisms that accomplish the motion of the vacancy through nearest neighbor jumps restoring order to the alloy at the end of the cycle. The traditionally postulated six-jump cycle is only one of the various cycles observed and some of these are quite complex. Diffusion at the grain boundary mainly takes place through sequences of coordinated nearest neighbor jumps yielding to a rearrangement of the grain boundary structure. Two distinct mechanisms resulting in a structural unit migration of the vacancy are also identified. The results are analyzed in terms of the activation and configuration energies calculated using molecular statics simulations.

ACKNOWLEDGEMENT

I would like to thank my advisor Dr. Diana Farkas, for giving me the opportunity to be introduced to the atomistic computer simulation world. Her patience, guidance and great help made this work possible. I also wish to thank Dr. Sean Corcoran and Dr. William Reynolds for serving on my committee.

Thanks to Clemmitt Sigler for his limitless availability and his kindness to answer my questions about UNIX.

For the pleasant atmosphere and their help, I wish to thank my office-mates and friends: Douglas Crowson and Antoine Latapie. Special thanks to Douglas for reading my manuscript and giving me helpful comments.

I am also thankful to Dr. Yuri Mishin for his help and contribution regarding to the Molecular Statics code used.

This thesis is dedicated to Marie Paule and Pierre Jacques Soulé de Bas, my parents, and also to the rest of my family.

Finally and most of all, I would like to thank Jacqueline for her support and understanding.

This work was sponsored by the National Science Foundation.

TABLE OF CONTENTS

LIST OF FIGURES

LIST OF TABLES

Chapter 1
INTRODUCTION

The B2 intermetallic compounds are of a great interest from both, a scientific and a technological point of view. They exhibit physical and mechanical properties that have been applied in many different areas including the aerospace and the micro electronic industries. Diffusion in these intermetallic compounds has been the subject of many theoretical and experimental studies over the past 50 years. The theoretical interest lies in the understanding of the different mechanisms of diffusion that can occur through the bulk or the grain boundary. From a technological point of view, many creep and sintering studies in intermetallic compounds are intimately connected with diffusion.

1.1 Bulk Diffusion in NiAl and other B2 Compounds

In most of the pure metal cases, the self-diffusion mechanism is well established and consists of nearest neighbor jumps (NN) where the atoms jump along a <1/2 1/2 1/2>-a vector type (a is the lattice parameter), as illustrated in Figure 1.1. The diffusion in B2 compounds is much more complex. This complexity arises because of the ordered structure and the additional energy involved in any mechanism that would destroy order, even if only temporarily. Two main categories of mechanism have been postulated to characterize the diffusion in B2 compounds. The first type of mechanisms involves next nearest neighbor jump (NNN), where the atoms jump along a <1 0 0>-a vector type (see Figure 1.2). The second type of mechanism refers to cyclic mechanisms, where the atoms perform a series of nearest neighbor jumps following a definite path.

The next nearest neighbor jump mechanism implies that the atoms jump in their own sublattice, in a second neighbor site. This mechanism can be expected as energetically favorable due to the fact that there is no disorder created during the process.

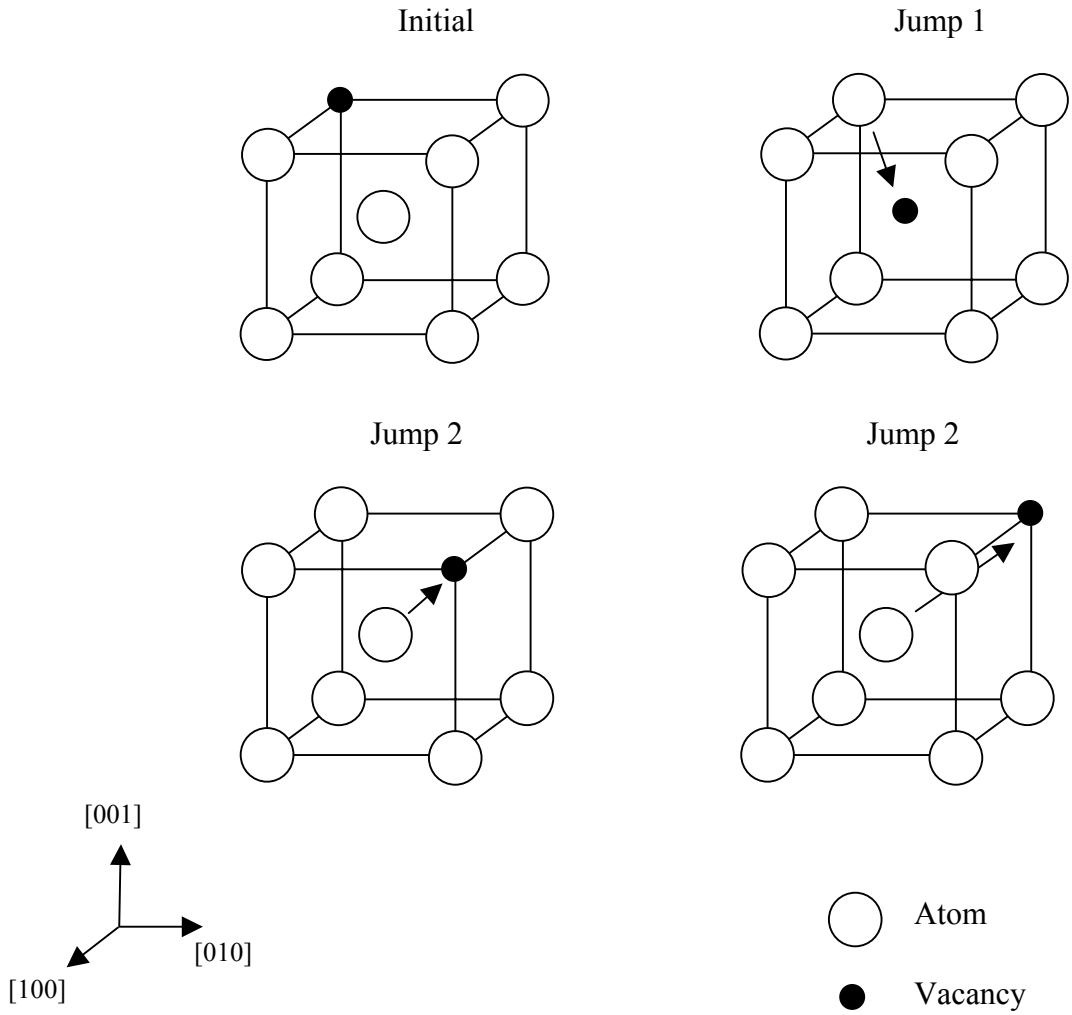

Figure 1.1: Graphical representation of [110] and [010] vacancy migrations via nearest neighbor jumps.

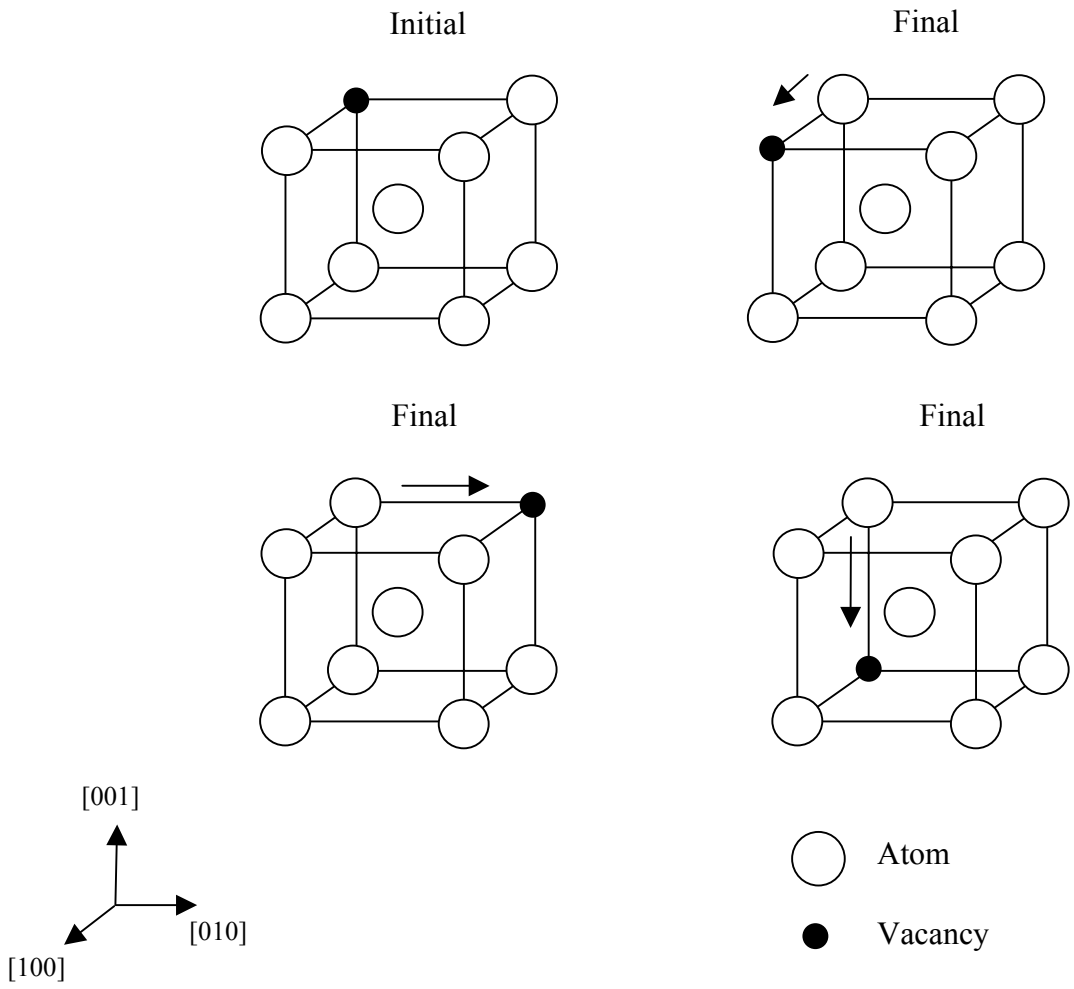

Figure 1.2: Graphical representation of [100], [010], and [$00\bar{1}$] vacancy migrations via next nearest neighbor jumps.

Thus, Donaldson and Rawlings [1], based on a study of a diffusion tracer, suggested a NNN mechanism for the Ni atoms in the NiGa B2 compound. Without excluding the possibility of some nearest neighbor jumps, the absolute values and compositional dependence of the Ni diffusion coefficient D_{Ni} and the activation energy of Ni, Q_{Ni}, are consistent with Ni diffusion occurring mainly via next nearest neighbor jumps. Lutze-Birke and Jacobi [2], based on the investigation of the diffusion of ^{114m}In in NiAl B2 compound, obtained frequency factor values D_0 suggesting that the diffusion occurred via next nearest neighbor jumps. A similar investigation, done by Hahn et al. [3], on the intermetallic B2 electron compound PdIn yielded similar results. The high ordering energy values found suggested that the diffusion occurred at low temperature via next nearest neighbor in PdIn. More recently, Mishin and Farkas [4] used molecular statics simulations with EAM potentials to determine the activation energies of different diffusion mechanisms in a NiAl B2 compound. Based on the used potentials, the results suggested that the NNN is energetically favorable in stoichiometric NiAl.

The nearest neighbor jump mechanism can be argued to be less favorable because the atoms initially jump to the wrong sublattice, creating partial disorder in the crystal in the form of antisites. Several mechanisms have been suggested where the partial order is recovered after a certain number of nearest neighbor jumps, constituting a diffusion cycle. The best known of these is the 6-jump cycle, postulated by Elcock and McCombie [5], where the vacancy migrates along a definite path of 6 nearest neighbor jumps. After the six jumps, the order in the crystal is restored and the vacancy has migrated as a result of the cycle. Figure 1.3 illustrates a 6-jump cycle occurring in a {110}-type plane in a B2 NiAl. There are three basic types of the 6-jump cycle proposed. The first one is a cycle that is entirely contained in a {110}-type plane and the vacancy migrates by a <110>-type vector. In the second type, the vacancy migrates by a <100>-type vector and the entire cycle is still contained in a {110}-type plane. This is called the straight [100] cycle. The last type is a cycle in which the vacancy migrates by a <100>-type vector and the cycle is not contained in a single {110}-type plane. This is called a bent [100] cycle. The three types of 6-jump cycles described above are illustrated in Figure 1.4. Since this cyclic mechanism was first proposed in 1958, it has been widely accepted as a main diffusion mechanism in ordered alloys. Wynblatt [6], using early computational

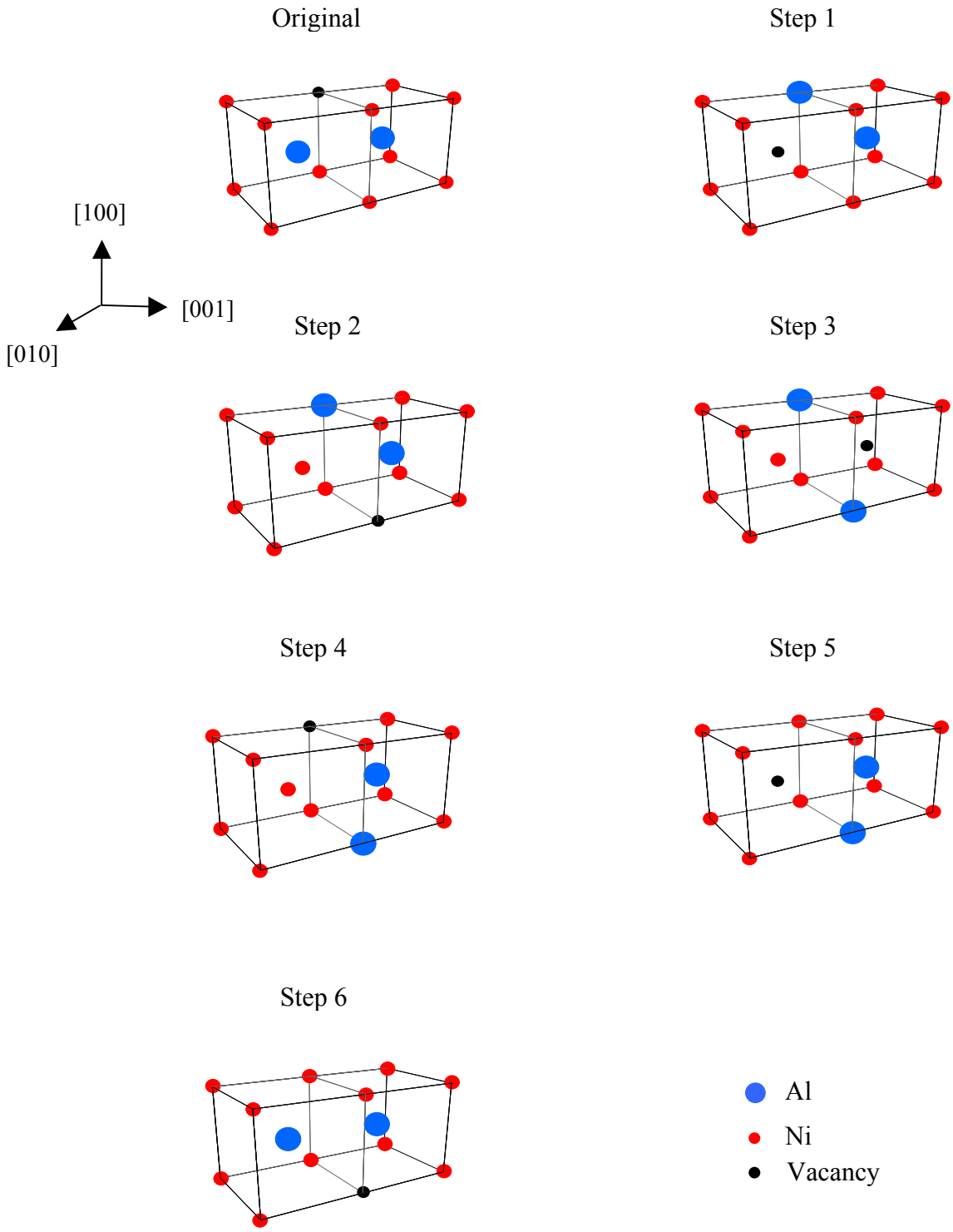

Figure 1.3: Graphical representation of a [110]-6JPC in B2 NiAl.

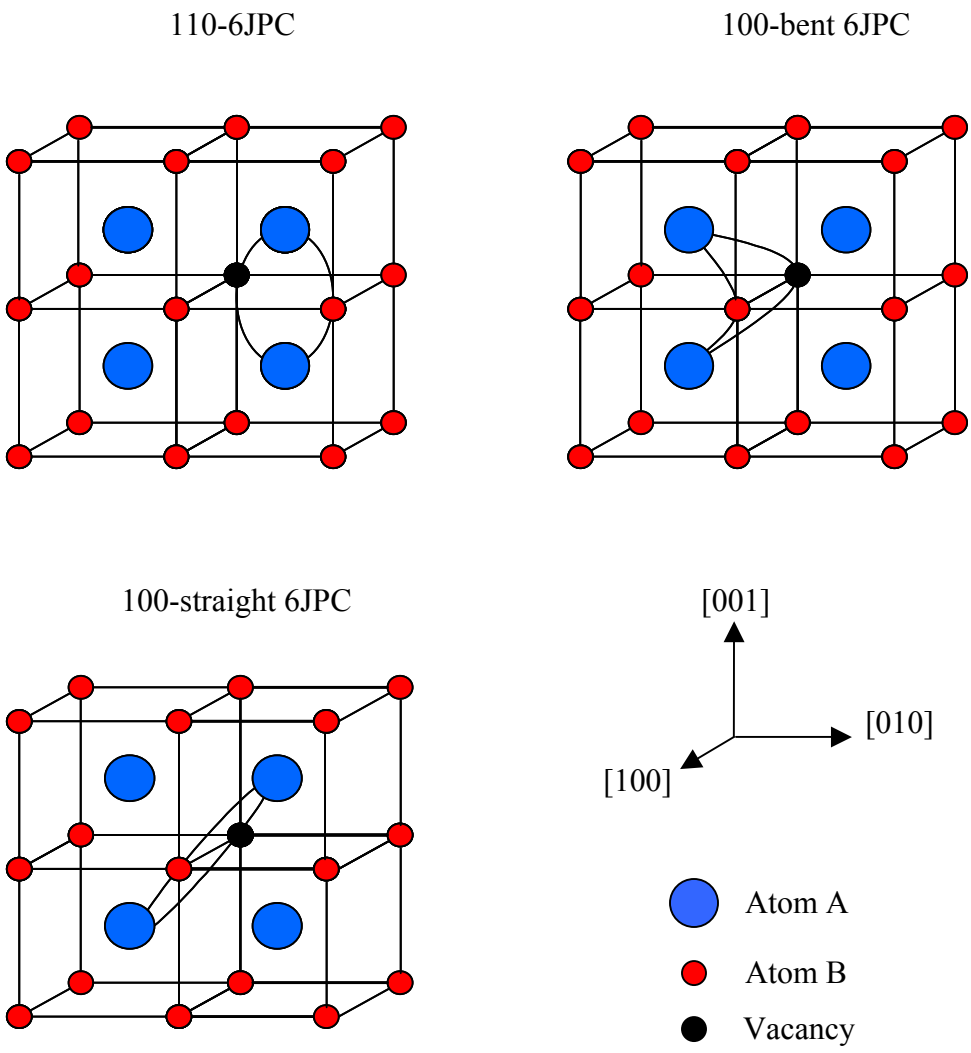

Figure 1.4: Graphical representation of the three different types of 6JPC in a B2 structure.

techniques, studied the defect migration energies in β-AgMg by 6-jump cycle, by next nearest neighbor jumps and by divacancy migration. Based on the modified Morse potentials, the 6JPC was found to be, energetically, the most favorable. More recent investigations done by Belova et al. [7], based on a Monte Carlo simulation investigation of the tracer correlation factor and the cosines of the angle between consecutive tracer jumps, suggested that the 6JPC is dominant in the case of an ordered alloy. Studies based on a statistical thermodynamic treatment of point defects in B2 intermetallic compounds [8] show the 6JPC is operative near the stoichiometric composition. Drautz and Fähnle [9], based on two different modeling techniques, the mean-first-passage time concept formally used by Arita et al. [10] and a rate equation method introduced by Ishioka and Koiwa [11], determined the ratio P_{110}/P_{100} of the probabilities for effective jumps via [100] cycles or via [110] cycles. These two methods yielded very similar results at low temperature ($T<2400$ K), where P_{110}/P_{100} varies from ≈ 0.33 to 0.36. Experimental studies done with quasi-elastic Mössbauer spectroscopy (QMS) [12] and nuclear resonant scattering (NRS) [13] on FeAl showed that the diffusion of Fe in the B2 phase takes place via NN jumps. Theses investigations did not yield to an obvious diffusion jump mechanism for the Fe diffusion in FeAl, but the P_{110}/P_{100} values being respectively 1.7 in reference [12] and 1.9 in reference [13] are seen to be in conflict with Drautz and Fähnle [9]. However, a Monte Carlo simulation investigation [14] based on QMS/NRS experiments [12, 13] showed that these results are compatible with a diffusion mechanism based on the 6-jump cycle. Similarly to [12, 13], studies done using nuclear neutron scattering [15] on NiGa showed that the Ni atoms diffuse via NN jumps.

Several additional mechanisms have been postulated to describe the diffusion in B2 intermetallic compounds. However, most of these mechanisms are relevant to more complex initial alloys that contain more point defects, are non-stoichiometric and partially ordered. Thus, Wynblatt [6], in his study of the defect migration energies in β-AgMg, considered a divacancy diffusion mechanism. Figure 1.5 represents a system with two vacancies in two nearest neighbor sites in an ordered AB B2 compound. The divacancy mechanism consists of an A atom jumping directly to a next nearest neighbor site. In the configuration described in figure 1.5, the energy required to proceed to the NNN jump is lowered by the missing B atom that would constitute the saddle point (the

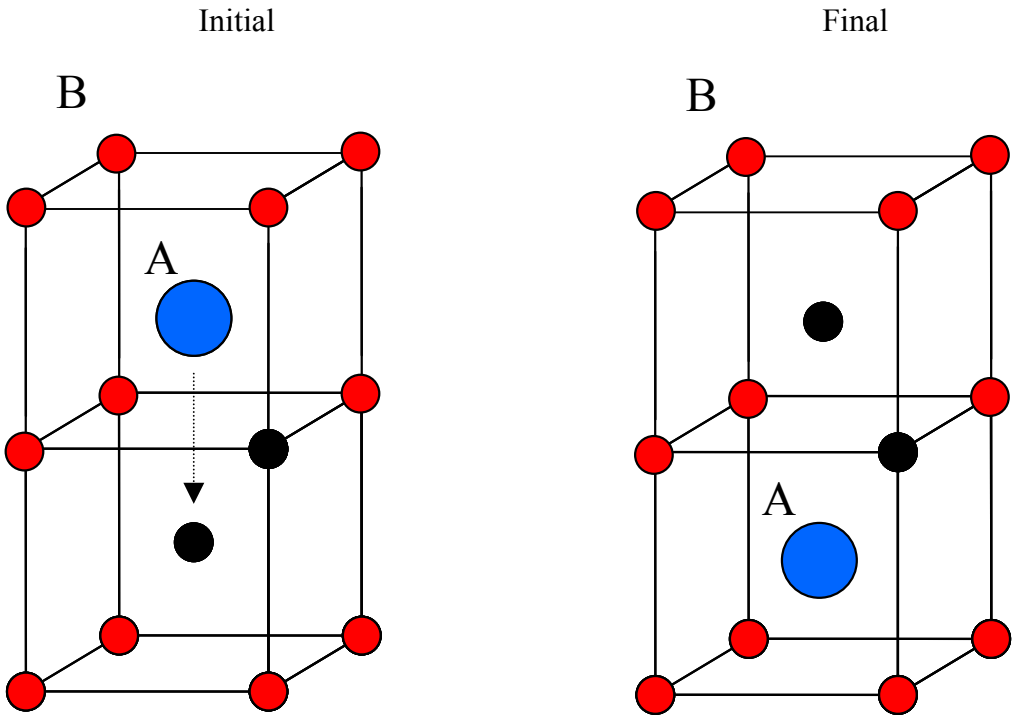

Figure 1.5: Graphical representation of the divacancy mechanism.

high energy configuration) for the A jumping atom. Stolwijk et al. [16], based on the study of both diffusion tracers ^{60}Co and ^{67}Ga in CoGa B2 compounds, introduced the triple defect mechanism as an alternative to the 6-jump cycle. The triple defect, illustrated in step 1 figure 1.6, corresponds to a configuration where one A atom has performed a nearest neighbor jump, being now an anti-structure atom, and where the two vacancies belong to the same sublattice at a next nearest neighbor distance. When the anti-structure A atom jumps further in its sublattice (see step 2 in fig. 1.6), the final configuration is equivalent to the final configuration of a divacancy mechanism where the lattice remains ordered. Athènes et al. [17], studying the atom migration resulting from exchanges with a single vacancy by Monte Carlo simulation, presented the antisite-assisted 6-jump cycle mechanism (A6JPC). This mechanism consists of a classical 6-jump cycle where the presence of an antisite in a next nearest neighbor site of the vacancy lowers the activation energy barrier. This antisite is not involved in any exchange with the vacancy in the 6-jump cycle. Figure 1.7 represents the initial and the final configurations of a [110]-A6JPC. Kao and Chang [18], in a thermodynamic analysis in terms of specific point defects in intermetallic B2 compounds, introduced a new mechanism, the anti-bridge structure (ASB). This mechanism is related to non-stoichiometric alloys where the concentration of anti-structure atoms is sufficiently high to constitute a bridge through which the vacancy can migrate. As illustrated in figure 1.8, a vacancy can migrate, within the same unit cell, to a first next nearest neighbor site (nnn in fig. 1.8), to a third nearest neighbor site (n4 in fig. 1.8), or to a fifth nearest neighbor site (n5 in fig. 1.8), all these next nearest neighbor jumps consist of two nearest neighbor jumps. This mechanism does not involve any extra disorder of the lattice, the B atoms remaining in the same position (see fig.1.8). Kao and Chang showed, in their investigation, that the ASB mechanism becomes important at large deviation from stoichiometry.

The goal of this present work is to observe the diffusion mechanisms in B2 ordered compounds by direct Molecular Dynamics. The B2 compound is simulated as an initially homogeneous alloy of stoichiometric composition, into which one vacancy is introduced. The diffusion events observed in the MD simulations are reported as a function of their natures, and these results are then correlated with corresponding

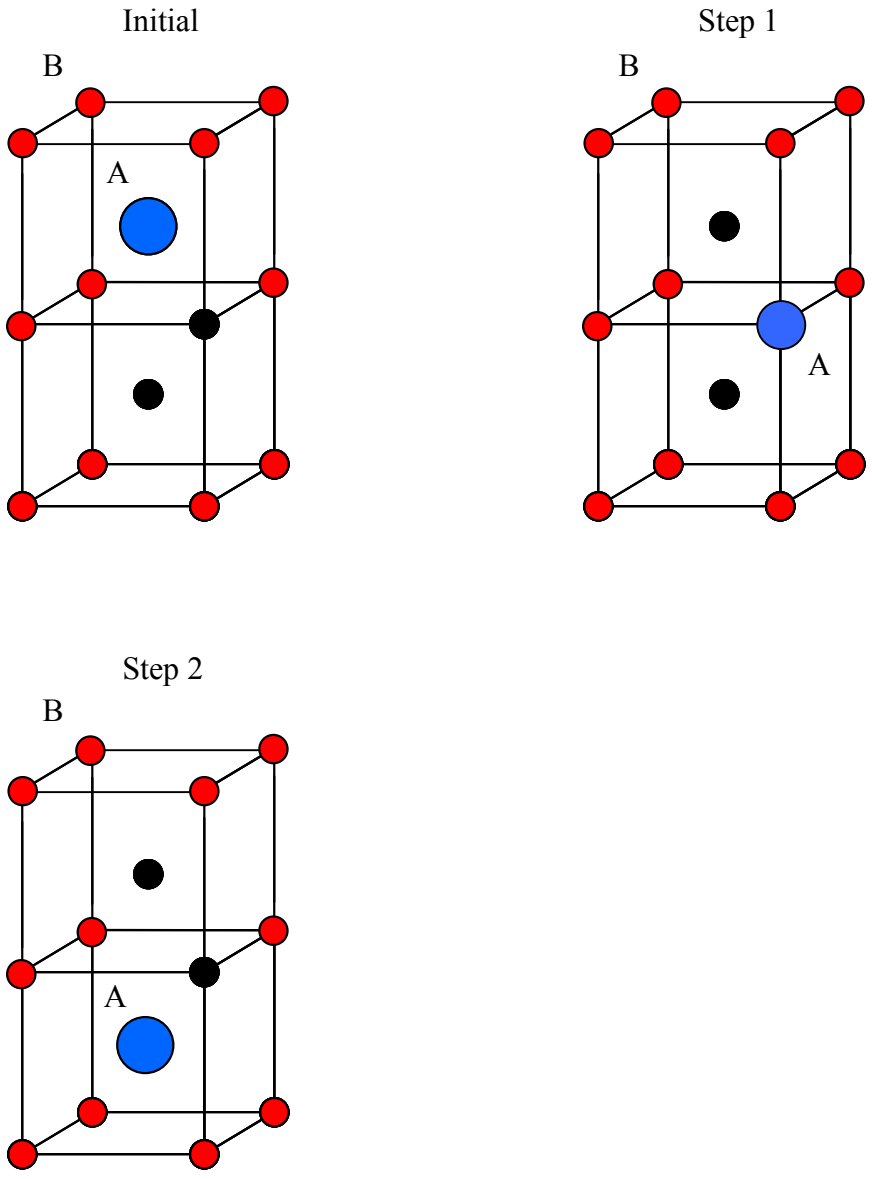

Figure 1.6: Graphical representation of the triple defect mechanism.

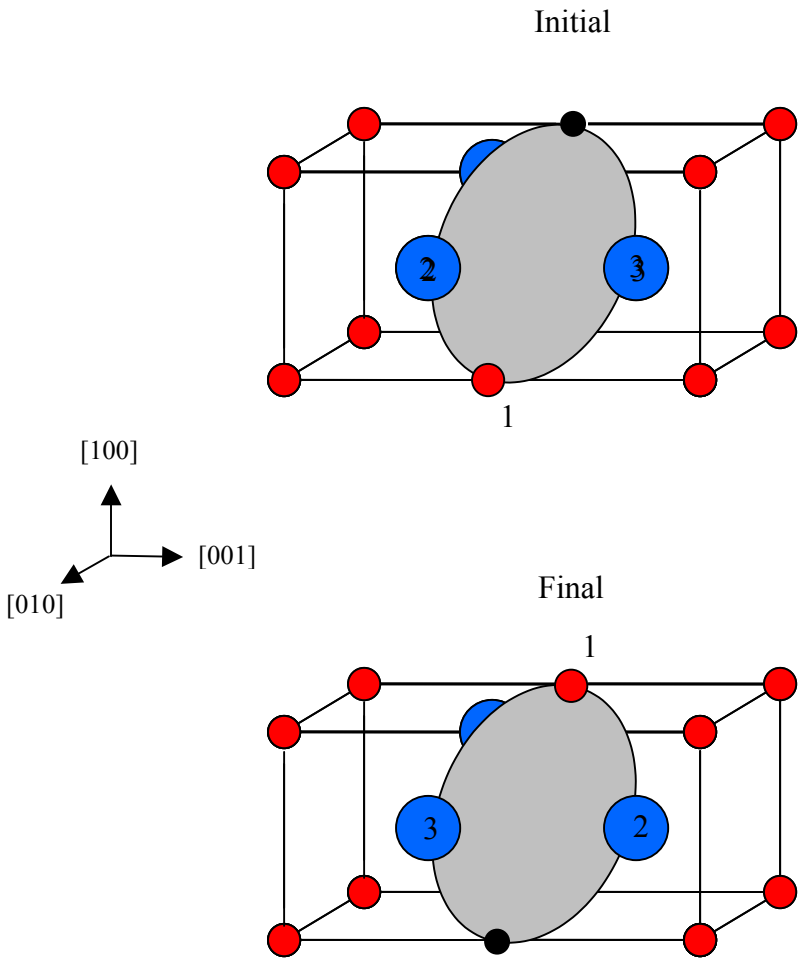

Figure 1.7: Graphical representation of the initial and final states of a [110]-6AJPC in a B2 compound.

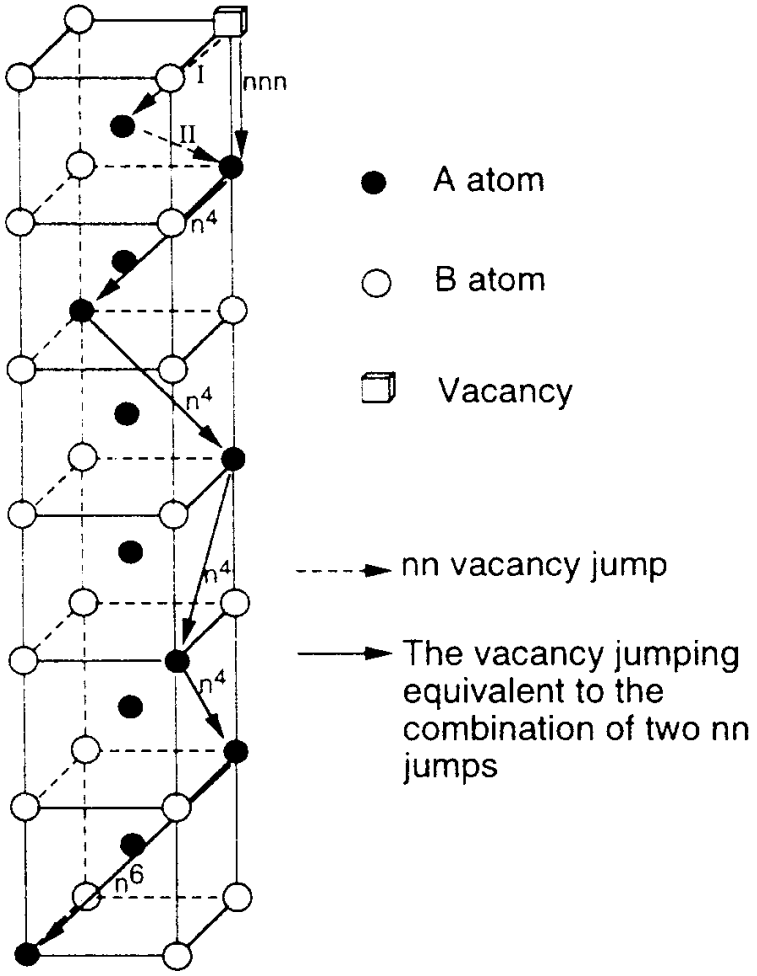

Figure 1.8: Graphical representation of the Anti-Structure Bridge mechanism. After Kao and Chang [18].

activation energies calculated by Molecular Statics. Embedded Atom Method (EAM) potentials developed to fit the B2 NiAl properties are used in the simulations.

1.2 Grain Boundary Diffusion

Grain boundaries are known to contribute to faster diffusion than in the bulk by providing an easy path for matter transport. Unlike the bulk structure where every site is equivalent, the grain boundary structure exhibits distinct sites in the GB core that will be more favorable to diffusion than other sites. The temperatures for which diffusion can be observed in direct MD are expected to be lower when it occurs through the grain boundary rather than in the bulk.

As with the bulk diffusion, grain boundary diffusion has been the subject of several types of investigations over the past fifty years, mainly on pure metals (Ag, Au, Cu) and intermetallic compounds (NiAl). The two most widely studied grain boundary structures are the pure tilt boundaries and the pure twist boundaries, for which the misorientation between the grains is obtained through rotation around axis that is either perpendicular or parallel to the grain boundary plane, respectively. Whereas structural analyses [19, 20] are focused on structure energy calculations for various grain boundaries, diffusion-oriented investigations tend to study the influence of the structure on the diffusion process. Another widely developed area of investigation is the determination of values for specific data characterizing the diffusion, such as the diffusion coefficient D_{gb} or the correlation factor f_{gb}. Contrary to diffusion in the bulk, where the main mechanisms have been postulated and intensively studied, the atomistic mechanisms of GB diffusion are still poorly understood. Due to the limitations of the experimental techniques and the additional constraints imposed by the orientations of the grain boundary structures, computer simulations represent an appropriate tool that is widely used.

Early experimental investigation [21] on grain boundary diffusion was performed on [100] tilt boundaries in Ag. The diffusion coefficients relative to the diffusion parallel and perpendicular to the tilt axis, $D_{gb}^{//}$ and $D_{gb}^{\perp}$ respectively, were determined in function

of the misorientation of the grain boundary. For small angle misorientation, the diffusion takes place mainly along the direction parallel to the tilt axis, with $D_{gb}^{//} = 15 x D_{gb}^{\perp}$. For larger values of misorientation angle (tilt angle $\theta \approx 45°$) the ratio $D_{gb}^{//} / D_{gb}^{\perp}$ is found to drop to 2. In a more recent investigation [22] performed on [110] tilt boundaries in Ag, Sommer et al. report results that are in conflict with the Hoffman's investigation [21]. By use of the tracer technique (^{105}Ag-tracer), the determination of the diffusion coefficient showed a $D_{gb}^{//} / D_{gb}^{\perp}$ ratio that is relatively constant and equal to 2-3 over the range of tilt angle studied (θ varying from 0° to 90°). Contrary to reference [21], the diffusion anisotropy measured in this investigation [22] is relatively small and independent of the tilt angle. The evolution of grain boundary diffusion with the orientation has also been the subject of several investigations. In an investigation similar to reference [21], Turnbull and Hoffman [23] studied [100] tilt grain boundaries in Ag. For small angle boundaries, a continuous behavior of the diffusivity is found. Ma and Baluffi [24], using a newly developed surface accumulation method, studied Ag diffusion along the tilt axis of a series of [001] tilt boundaries in the Ag/Au system. δD_{gb} (δ the width of the grain boundary) was measured for sixteen grain boundaries as a function of the temperature and the tilt angle (θ varying from 15° to 85°). The activation energy was deduced from an Ahrenius diagram, and reported as a function of the tilt angle. Figure 1.9 shows the obtained diffusion parameter δD_{gb} at 190°C. The diffusion parameter is seen to increase monotonically with increasing tilt angle, reach a maximum around $\theta = 45°$, and then decrease monotonically. This result is in agreement with reference [23] for the low-angle range. Figure 1.10 shows the results of the activation energy as a function of the tilt angle. The activation energy is a fairly smooth function of the tilt angle. It decreases slightly when the structure changes from low-angle to high angle. Budke et al. [25] have recently studied the self and Au-impurity diffusion in several Cu grain boundaries having tilt angles in a range of 6° about the ideal Σ 5(310)[001] angle. By using the two diffusion tracers ^{64}Cu and ^{195}Au, $s\delta D_{gb}$ (s is the segregation factor of the grain boundary) was determined as a function of the temperature for each grain boundary. The activation energies relative to the given tilt angles were then deduced from the Arhenius diagram. This investigation showed that for both self-diffusion and impurity diffusion, the diffusivity exhibited a well-defined minimum and the activation energy a maximum for a

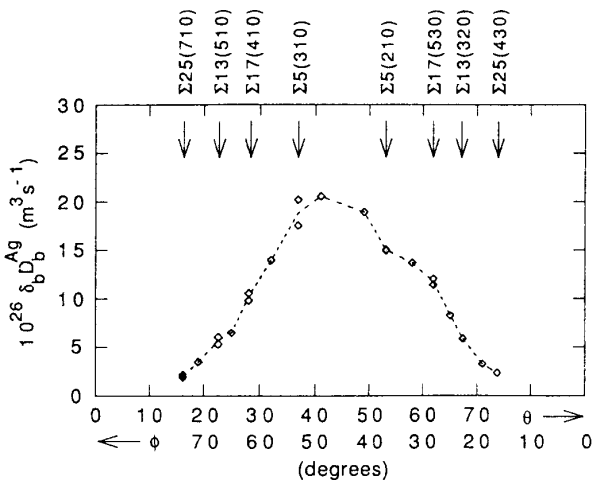

Figure 1.9: Measured grain boundary diffusion parameter $\delta_b D^{Ag}_b$ as a function of tilt angle θ (or φ) at 190°C. After Ma and Baluffi [24].

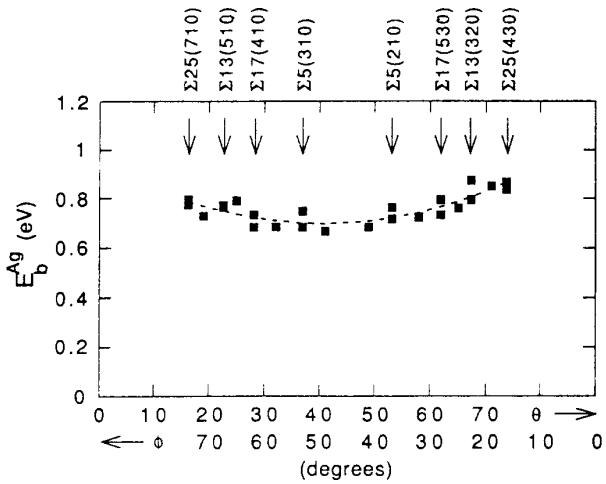

Figure 1.10: Measured activation energy E^{Ag}_b as a function of a tilt angle. After Ma and Baluffi [24].

tilt angle value slightly below the ideal value $\theta_{\Sigma 5(310)[001]}$. This result is in conflict with the conclusions drawn in references [23, 24] and suggests that a very focused analysis is necessary to characterize its influence on diffusion. The correlation factor has been the subject of several investigations. Mishin [26], by use of specific Monte Carlo calculations, studied the migration of diffusion tracer in a 5(310)[001] Ag tilt grain boundary. The correlation factors by vacancy mechanism parallel and perpendicular to the tilt axis were determined as a function of the temperature.

Most of the studies dedicated to the analysis of the diffusion mechanisms at the grain boundary are focused on the two main categories of diffusion mechanisms: the vacancy-related mechanisms, were the atoms jump via vacant sites, and the interstitial mechanisms, where the atoms jump in interstitial lattice sites. In an early computational investigation performed with Molecular Dynamics, Kwok et al. [27] studied the diffusion in a Σ 5(310)[001] Fe tilt boundary. The results of this study indicate that the diffusion occurs via a vacancy-related mechanism. In the range of temperatures that are significant to the diffusion, the formation of interstitials is seen to occur with increasing temperatures, but is not promoting self-diffusion. Liu and Plimpton [28], in Molecular Statics and Molecular Dynamics investigations of diffusion along [001] tilt grain boundaries, studied the influence of temperature on the diffusion mechanism involved. MS calculations are used to determine the activation energies of the different possible paths for diffusion in the low-temperature regimes, whereas MD simulations describe the diffusion at high-temperature regime. The two techniques were applied to Σ 5(310)[001] and Σ 13(320)[001] tilt grain boundaries with an EAM potentials developed to fit Ag properties. The results of this study show that the interstitial mechanisms are dominant at low temperature whereas the vacancy-related mechanisms become dominant at high temperature, due to increase vacancy concentration and mobility. Nomura and Adams [29] performed a Molecular Statics analysis similar to [28] on six different (100) twist grain boundaries, to investigate the influence of twist angle on the diffusion mechanism. EAM potentials were used to simulate Cu. The activation energy values found reveal that the interstitial mechanisms are favored for high angle boundaries, and that vacancy related mechanisms are favored for low angle boundaries. This trend is explained in terms of volume expansion of the grain boundary that makes the formation and the

migration of interstitials easier for high angles. More recently, Sørensen et al. [30] used Molecular Dynamics combined with Kinetic Monte-Carlo (KMC) simulations to perform a more focused analysis on the diffusion mechanism at two Σ 5[001] Cu tilt boundaries. The grain boundaries were studied at the atomic scale and diverse mechanisms involving distinct sites of the GB core were investigated. Both vacancy-related mechanisms and interstitial mechanisms were considered in this study. Figure 1.11 illustrates the different vacancy-related mechanisms reported in this investigation for the Σ 5(310)[001] Cu GB. The distinct sites within the GB core are identified by distinct numbers, and the different vacancy or interstitials migrations are reported by arrows. The vacancy transitions shown are mainly simple atom-vacancy exchange where atoms located in 1', 2, 4, and 5 jump into site 1 (see fig. 1.11). This study also reports a specific transition, 1 6 $\widetilde{4}$, where atom 6 jumps towards site 1 and atom 4 jumps towards the vacant site left by atom 6. This can be seen as a long-range vacancy diffusion perpendicular to the tilt axis where the vacancy migrates to a neighboring structural unit. Figures 1.12(a) and 1.12(b) illustrate the different interstitial mechanisms reported in this investigation for the Σ 5(310)[001] GB. Diffusion parallel to the tilt axis occurs via a I 1 I* transition (I* being a <100> vector translation of I), where I kicks atom 1 out to site I* and takes its place, as illustrated in figure 1.12(a). Diffusion along the tilt boundary, in the $[1\,\bar{3}\,0]$ direction, occurs via the transition I 2 $\widetilde{3}$ $\widetilde{I}$, as reported in figure 1.12(a), or via the transition I 2 $\widetilde{6}$ $\widetilde{1}$ $\widetilde{I}$ reported in figure 1.12(b). In both cases, the interstitial is seen to migrate to a neighboring structural unit. This investigation also highlighted the influence of the grain boundary structure on the diffusion mechanism as well as the influence of the temperature on the correlation factor.

In the present work, a Molecular Dynamics investigation is performed to determine the different diffusion mechanisms occurring at a Σ5(210)[001] grain boundary in B2 compounds. Vacancies are introduced into specific Ni sites within the core structure of a low energy Σ5(210)[001] grain boundary. The results of the MD simulations are reported as a function of the initial configuration and analyzed in terms of configuration energies calculated by Molecular Statics. The EAM potentials used for this GB investigation are the same as those used for the bulk simulations.

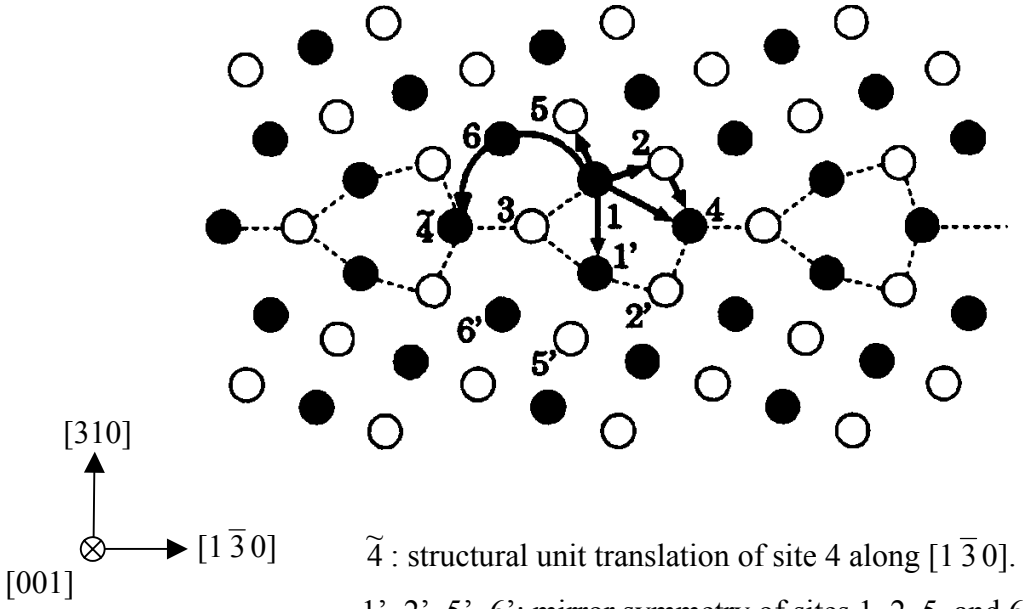

$\widetilde{4}$: structural unit translation of site 4 along [1 $\bar{3}$ 0].

1', 2', 5', 6': mirror symmetry of sites 1, 2, 5, and 6 across (310).

Figure 1.11: Vacancy transitions in a Σ 5(310)[001] grain boundary. After Sørensen et al. [30].

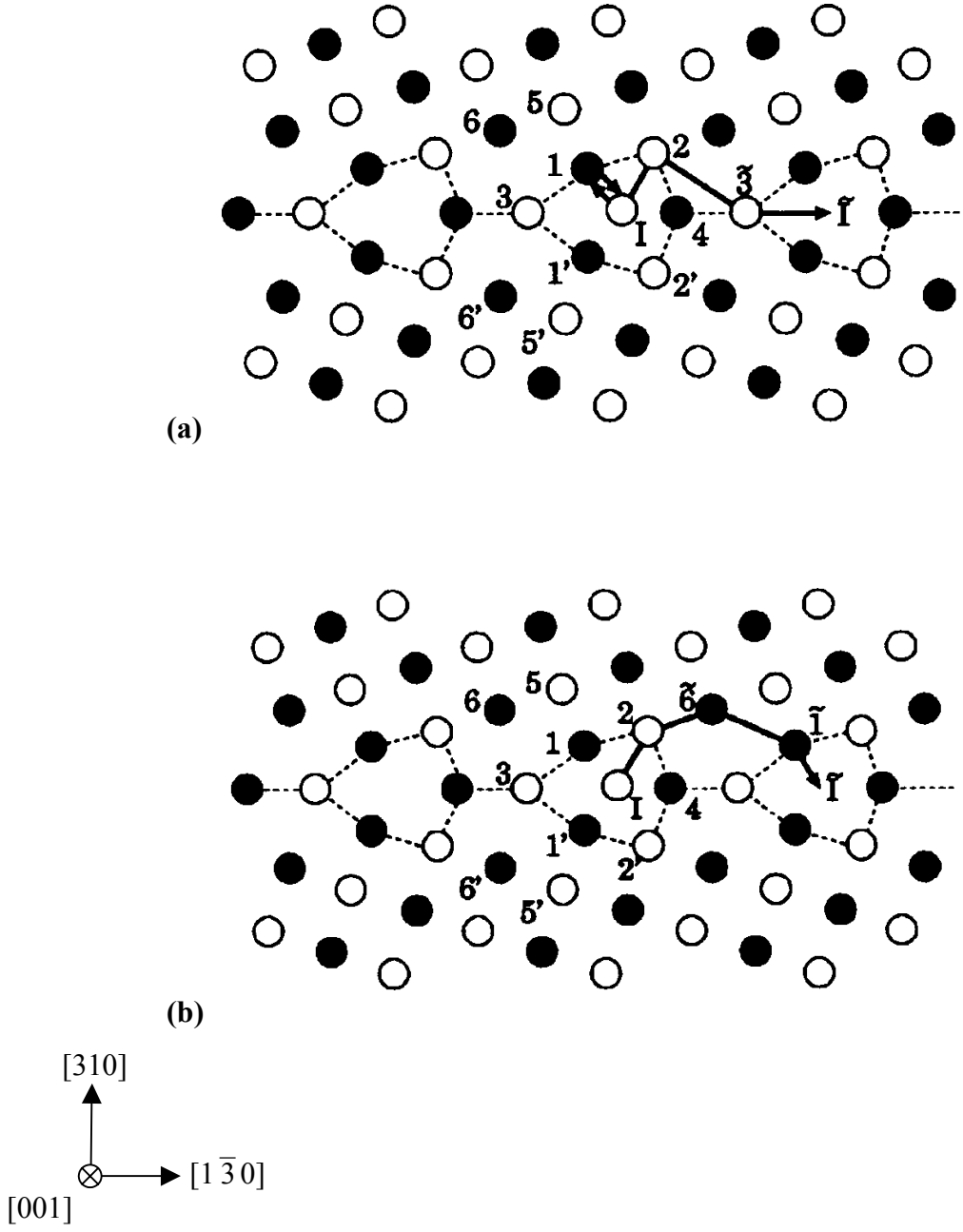

Figure 1.12: Interstitialcy transition in a Σ 5(310)[001] grain boundary. After Sørensen et al. [30].

Chapter 2
ATOMISTIC SIMULATION TECHIQUE

The use of computer simulation techniques is becoming more and more important in the understanding of the microscopic behavior of materials. Whereas a general and macroscopic characterization of materials can be obtained by experiments, computer simulations, designed by reproducing materials properties, provide insight into their behaviors at the atomic scale. With the sophistication of the atomistic simulation methods and the increase of computational power, a more accurate description of the interatomic interactions in crystalline materials can be developed. Radically opposite approaches, such as the Monte Carlo (MC) [31] or the Molecular Dynamics [32] methods, have been developed over the past fifty years. Each technique yields to different types of analysis, giving different types of results. While MC, considered as a stochastic process, provides data such as diffusion coefficient or correlation factor, MD, considered as a determinist process, characterize the overall and physical behavior of the system.

Because of the actual situation of the experimental techniques that do not allow an accurate description of the diffusion mechanisms, the computer simulations represent an appropriate tool. The present study was conducted with Molecular Statics and Molecular Dynamics calculations using embedded atom interatomic potentials.

2.1 Molecular Dynamics Simulation

2.1.1 Equation of Motion

The behavior of a system of particles, including both electron and nuclei, can be determined by solving the time-dependent Schrödinger equation. The accuracy required by this type of approach yield to very complex calculations that make its application to

the description of the system dynamics very difficult or even impossible. Whereas a quantum mechanics analysis seems delicate to compute, a classical mechanics approach is relatively straightforward and provides useful information. Thus, Molecular Dynamics is a technique that computes the equilibrium and the transport of a many particle-body by solving the equation of motion of the system.

If Newton's mechanics is sufficient to describe simple dynamics systems like atomics fluids, some more complex formulations such as the Lagrangian and the Hamiltonian [33] are necessary to deal with a more complex system. In the coming derivation, the Hamilton formulation is used to describe the fundamental concept of Molecular Dynamics.

The classical Hamiltonian, H, can be identified as the total energy of a system, the combined kinetic and potential energies. For a system of N spherical particles the Hamiltonian can be written as:

$$H(p_i, r_i) = \sum_{i=1}^{N} \frac{1}{2m_i} p_i^2 + U(r_i) \tag{1}$$

where p_i is the momentum of a particle i ($p_i = m_i . \dot{r}_i$, r_i being the position of the given particle and m_i its mass), and U is the effective potential. The Hamiltonian is a function of 6N independent variables, the 3 N momenta p_i and the 3 N particle positions r_i.
Considering an isolated system, the total energy E is conserved and the equation 1 is equal to a constant:

$$\sum_{i=1}^{n} \frac{1}{2m_i} p_i^2 + U(r_i) = E = Const \tag{2}$$

Considering the total time derivative of the general Hamiltonian (eqn.1) and a system that cannot exchange energy with its surrounding (eqn.2), one can derive equations of motion for the particles of the system similarly to reference [34]:

$$\dot{p}_i = -\frac{\partial H}{\partial r_i} = -\frac{\partial U}{\partial r_i} = f_i \tag{3.1}$$

and

$$\dot{r} = \frac{\partial H}{\partial p_i} = \frac{p_i}{m_i} \tag{3.2}$$

where f_i is the force applied to the particle i.

Substituting equation 3.2 in 3.1, the Hamiltonian formulation yields to Newton's second's law:

$$m_i \ddot{r}_i = f_i \tag{4}$$

Thus, Molecular dynamics consists essentially of integrating the equations of motions derived above via a numerical method. For very high accurate solutions of the equations of motion it is usually advantageous to solve a system of six first-order differential equations, as in the Hamiltonian approach (eqn. 3.1 and 3.2 applied in the three directions), rather than a system of three second-order differential equations as Newton's second law (eqn. 4 applied in the three directions).

Based on this approach MD can be seen as a simulation of a system that evolves over a period of time where its particles moves in phase space along their physical trajectories as determined by the equations of motion.

2.1.2 The Molecular Dynamics Method

The application of the MD concepts presented below is standard but constitutes a good illustration of the different codes used in MD simulations. The generic input file used in this study, reported in Appendix A, can be seen as a direct application of this coming description.

In a standard molecular dynamics simulation, general information about the system such as the number of atoms, the type, mass and atomic interactions are first defined. The initial configuration of the system, including the positions of the atoms and their initial velocities at the time t = 0, is then specified. The initial positions are obviously defined as a function of the crystallographic properties of the materials studied. The initial velocities are established as a function of a given initial temperature. Indeed, using a statistical thermodynamics approach, velocities can be computed from a temperature using the Maxwell-Boltzmann distribution. The value of the time step Δt, corresponding to the integration variable, also has to be assigned before the simulation

process starts. This value has to be low compared to the highest frequency motion to integrate accurately over the motions, but as large as possible to increase the length of the runs. The first step of the simulation corresponds to the calculation of the forces applied to the atoms at $t = 0$. Then, incrementing the value of Δt, the actual positions, forces and velocities are successively computed for $t = t + \Delta t$, in integrating the equation of motion defined by equations 3.1 and 3.2 (or eqn. 4). The displacements of the atoms and their energies can then be calculated for $t = t + \Delta t$. This process is repeated until the number of iteration chosen is reached.

The algorithm reported figure 2.1 illustrates the whole process described above.

2.1.3 Overview of the Technique

Molecular Dynamics simulation is a useful technique to compute the equilibrium and the transport properties of a classical system. Considering that the MD algorithm is directly derived from a classical mechanics treatment of the system, the given system is expected to evolve as it would evolve during experiments. The approach is therefore very similar to real experiments. The sample is first prepared with a given structure specific atomic interactions. Then the sample evolves constrained to the equations of motion until its properties do not change with time. Since the MD technique follows the actual forces on the atoms as they migrate, the diffusion mechanisms can be determined by direct observation, without having any *a priori* assumptions. The direct observations incorporate in a natural way correlation effects, entropy effects and other possible transformations in structure and/or mechanism that can occur with temperature. The relative importance of various mechanisms can also be studied as a result of the simulation. Thus, the MD simulation is a very powerful technique that yields to very detailed information about the simulated system. It is an appropriate tool when the goal is precisely study the exact nature of the diffusion mechanisms.

The Molecular Dynamics computer program used to perform this study is XMD. This program was written in C by Jon Rifkin [35]. It is designed for the simulation of

Molecular Dynamics algorithm:

- Composition of the system
    - Define the number of atoms
    - Define the type of atoms
    - Define the specific masses of atoms
    - Define the atomic interactions
- Initial values at $t = 0$
    - Assign the particles positions r_i
    - Assign the particles velocities v_i.
- Definition of a time step Δt
- Simulation Process
    - Initial force calculation at $t = 0$
        1. Calculate the position at $t + \Delta t$.
        2. Calculate the force at $t + \Delta t$.
        3. Calculate the velocities at $t + \Delta t$.
        4. Analysis that is required at $t + \Delta t$.
        5. Increment the time by Δt.
- Analyze the results.

Figure 2.1: Molecular Dynamics Algorithm

metals and ceramics. Different types of potentials such as Embedded Atom Method (EAM) potentials, pair potentials, Tersoff's silicon-carbon potential [36], or Stillinger-Weber's Silicon potential [37] can be used to simulate the interatomic interactions. XMD also performs static calculations but it has not been used in that purpose during this study.

2.2 Molecular Statics Simulation

Molecular Statics is a technique designed to determine the lowest energy configuration of a given system where a defect is introduced.

A three-dimensional simulation block is initially defined. Every atom within this block interacts with its surroundings as described by the given interaction potential. The presence of a defect induces forces on the atoms that are allowed to move in order to drive the system to a minimum energy configuration. This minimum energy state is reached through an iterative relaxation process. Using a conjugate gradient approximation method [38], the minimization technique moves the atoms along the direction of the steepest gradient of the energy function, i.e., in the direction of greatest energy decrease. In each single iteration step, the atom is displaced in the direction of the resultant force applied by its neighbors as well as in a direction perpendicular to its previous displacement. The energy is computed after each iteration and the system is assumed to be at equilibrium when the energy gradient drops to zero or when the forces on each atom are below a specified value. The number of iteration required to reach equilibrium may vary from several tens to several hundreds.

This technique is however limited by the lack of temperature effect considerations. No atomic vibration due to thermal activation are taken into account and the results obtained only characterize the material at 0 K.

The code used in this study was written in FORTRAN by Dr. Yuri Mishin [4].

2.3 Embedded Atom Interatomic Potentials

2.3.1 The Embedded Atom Method

The modeling techniques are improved to such an extent that the major deficiency remaining is the inaccuracy of the interatomic potentials used. It is then essential to construct reliable interatomic forces that can reproduce experimental data.

The Embedded Atom Method (EAM) is a recent approach used to simulate the interaction between atoms in metals and intermetallic compounds. It is based on the Hohenber-Kohn theorem [39], which states that the energy contribution of an atom on its surrounding neighbors is a function of the local electron density due to all the surrounding atoms. This approach becomes particularly important when point defects such as vacancy clusters, free surfaces, grain boundaries or dislocation cores are introduced and change the density in the materials. Based on the EAM approach, the interaction energies of the atoms are composed of two potentials functions. A classical pair interaction potential, V (Morse function), describes the attractive and repulsive electrostatic interaction between two atoms. An embedding function, F, takes into account the interaction energy of each atom with the local electron density associated with the neighboring atoms. Consequently, the total energy of the system is written as:

$$E = \frac{1}{2}\sum_{i,j} V(r_{ij}) + \sum_{i} F(\overline{\rho}_i) \tag{5}$$

with:

$$\overline{\rho}_i = \sum_{i} \rho(r_{i,j})$$

where ρ is the electronic density function, $\overline{\rho}_i$ is the density at atom i due to all its neighbors, and r_{ij} the interatomic distance between the atom i and j. The interaction energies are however only taken into account within a selected cut-off distance (usually a second closest neighbor distance) and considered as zero outside of this region. The embedding function $F(\overline{\rho})$ is determined by assuming that the crystal obeys Rose's equation of state [40], which scales the cohesive energy of most metals.

The embedding functions and the pair interaction potentials are generally designed to fit various physical properties of a system such as lattice constants, elastic constants, or formation energies of diverse defects. In a binary alloy, such as NiAl, seven functions are required to describe the system. V_{Ni-Ni}, F_{Ni}, ρ_{Ni} and V_{Al-Al}, F_{Al}, ρ_{Al} describes the properties of each pure metals Ni and Al. V_{Ni-Al} describes the atomic interactions between the atoms of Ni and Al, and is determined by fitting the properties of the binary alloy. Knowing the values of the different variables described above, the potential energy of the considered system is then calculated using equation 5.

The embedded atom method is however constrained to several types of limitations. Due to an angular dependence of the electron density that is not considered, the EAM technique failed to describe the interactions between covalent materials such as Si or Ge. The method is also limited in some cases where the Cauchy pressure, defined as $P=1/2\ (c_{12}-c_{44})$ (c_{12} and c_{44} being elastic constants), is negative. In this case, the elastic constants determined by EAM do not fit the values of the materials. Some more advanced techniques based on the EAM [41] have however been developed to overcome these limitations.

2.3.2 EAM Potentials for NiAl

The EAM potentials used in this study to simulate the NiAl B2 compound were developed by Farkas et al. [42]. The terms used to describe the interactions of each of the pure metals (V_{Ni-Ni}, F_{Ni}, ρ_{Ni} ,V_{Al-Al}, F_{Al}, ρ_{Al}) were the ones developed by Voter et al. [43], and the mixed interatomic potential (V_{Ni-Al}) was determined by fitting the thermodynamic and lattice parameter data, as well as the elastic constants and fault energies of different phases of the Ni-Al system. The angular dependence was not included. It is also important to highlight that the Cauchy pressure of NiAl is positive and the problem described in the previous section did not arise. Figure 2.2 shows the values predicted by the present potentials for various properties of the B2 NiAl. Other values predicted by the potentials of Voter et al. [43] and Rao et al. [44] are also reported.

Property	Experimental	Calculated	Calculated [43]	Calculated [44]
a (0.1 nm)	2.88	2.88	2.87	2.88
E_{coh} (eV)	4.50	4.49	4.38	4.43
C_{11} (eV/A^2)	1.24	1.16	1.74	1.18
C_{12} (eV/A^2)	0.85	0.77	1.15	0.79
C_{44} (eV/A^2)	0.72	0.77	1.11	0.80
APB (110)	—	286	340	425
APB (112)	—	340	410	499

Figure 2.2: Parameters for B2 NiAl given by EAM potentials. After Farkas et al. [42].

The potentials used in the present investigation have lately been modified by Mishin and Farkas [45]. In this new version of the potentials, the terms used to describe the interactions of each of the pure metals were adjusted to fit more accurately to diffusion data in pure Ni and Al. However, the mixed interatomic potential remained the same as in the original version of the potentials [42]. For the present study we used the first version of the potential that has a lower activation energy, therefore allowing better statistics in the times that can be realistically reached in direct molecular dynamics.

Chapter 3
DIFFUSION IN THE BULK

3.1 Molecular Statics Investigation

Besides the Molecular Dynamics investigation, a Molecular Statics analysis is performed to determine the activation energies of the various diffusion mechanisms expected to take place in the bulk diffusion. Referring to the literature (see chapter 1), the diffusion via next nearest neighbor and via 6-jump cycle are seen to be the two most common mechanisms involved. In the following section, the activation energies are calculated for the 6-jump cycle and the next nearest neighbor jump for both point defect migration: a Ni and Al vacancy.

3.1.1 Computational Procedure

The curves of the migration energy of the vacancy are obtained by a simple energy minimization technique in a molecular statics framework (see section 2.2). Essentially, to determine the migration energy of a vacancy, one of it neighboring atoms is moved towards the vacant site in small steps and the total energy of the simulation block is minimized with respect to displacements of all other atoms. The jumping atom itself is also allowed to relax in directions perpendicular to the jump direction, but not in the jump direction. The minimum energy is obtained as a function of the atomic displacement along the jump vector. The maximum in this curve represents the saddle-point energy. This energy minus its initial energy before the jump is identified as the vacancy migration energy.

This technique is applied for both, NNN vacancy jumps within the same sublattice as well as to NN vacancy jumps involved in 6-jump cycles. In the latter case the locus of equilibrium positions of the jumping atom did not generally coincide with a straight line connecting the initial and final positions and the saddle point may be shifted from the midway point toward either the initial or final position.

The simulations were performed on a cubic block with dimensions 9a×9a×9a. The atomic interaction is described by the EAM potential [42].

3.1.2 Activation Energy Results

The activation energies for a next neighbor jump were obtained using the molecular statics method. Table 3.1 shows the calculated vacancy formation energy, E^f, (independent of the mechanism), the effective vacancy migration energy, E^{meff}, and the activation energy of self-diffusion, Q, for the next nearest neighbor vacancy mechanism in NiAl. The activation energy is obtained by adding the vacancy formation energy and the effective vacancy migration energy. The effective migration energy and activation energy for the Ni diffusion are E_{Ni}^{meff}=2.07 eV and Q_{Ni}=2.75 eV respectively. For the Al diffusion these values are E_{Al}^{meff}=1.70 eV and Q_{Al}=2.93 eV respectively. The activation energy value calculated for the Ni diffusion is consistent with the experimental values determined by Hancock and McDonnel [46], Q_{Ni}=3.18±0.1 eV, and by Divinski and Herzig [47], Q_{Ni}=3.01±0.04 eV. Based on the results reported in table 3.1, even if the effective migration energy of an Al vacancy is lower than the effective migration energy of a Ni vacancy, Al is expected to diffuse, via next nearest neighbor jump, more slowly than Ni. Indeed, the Al activation energy is slightly higher than that for the Ni vacancy.

The migration energies for the [110] 6-jump cycles are reported in Figure 3.1 and Figure 3.2, in form of an energy-displacement curve. In both cases, the highest migration energy corresponds to the third jump. For the Ni diffusion, the highest migration energy is E_{vNi}^{meff}=1.34 eV. For the Al vacancy diffusion, the highest migration energy is E_{vAl}^{m}=1.32 eV, while the effective vacancy migration (value of the curve maximum in

Table 3.1: Calculated vacancy formation energy, vacancy migration energy and the activation energy of self-diffusion (Q) for the next nearest neighbor vacancy mechanism in NiAl.

	Formation energy (eV)	Migration energy (eV)	Activation energy (eV)
Ni diffusion	0.68	2.07	2.75
Al diffusion	1.23	1.70	2.93

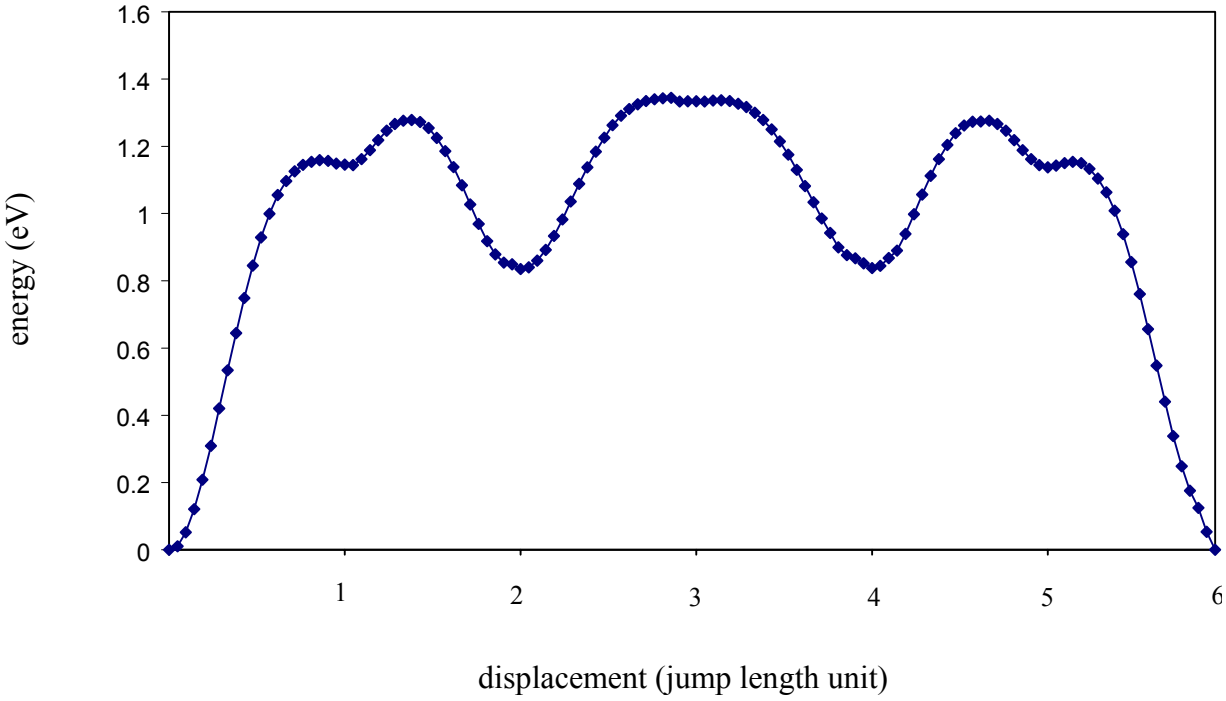

Figure 3.1: Energy-displacement curve for a [110] 6JPC in Ni vacancy.

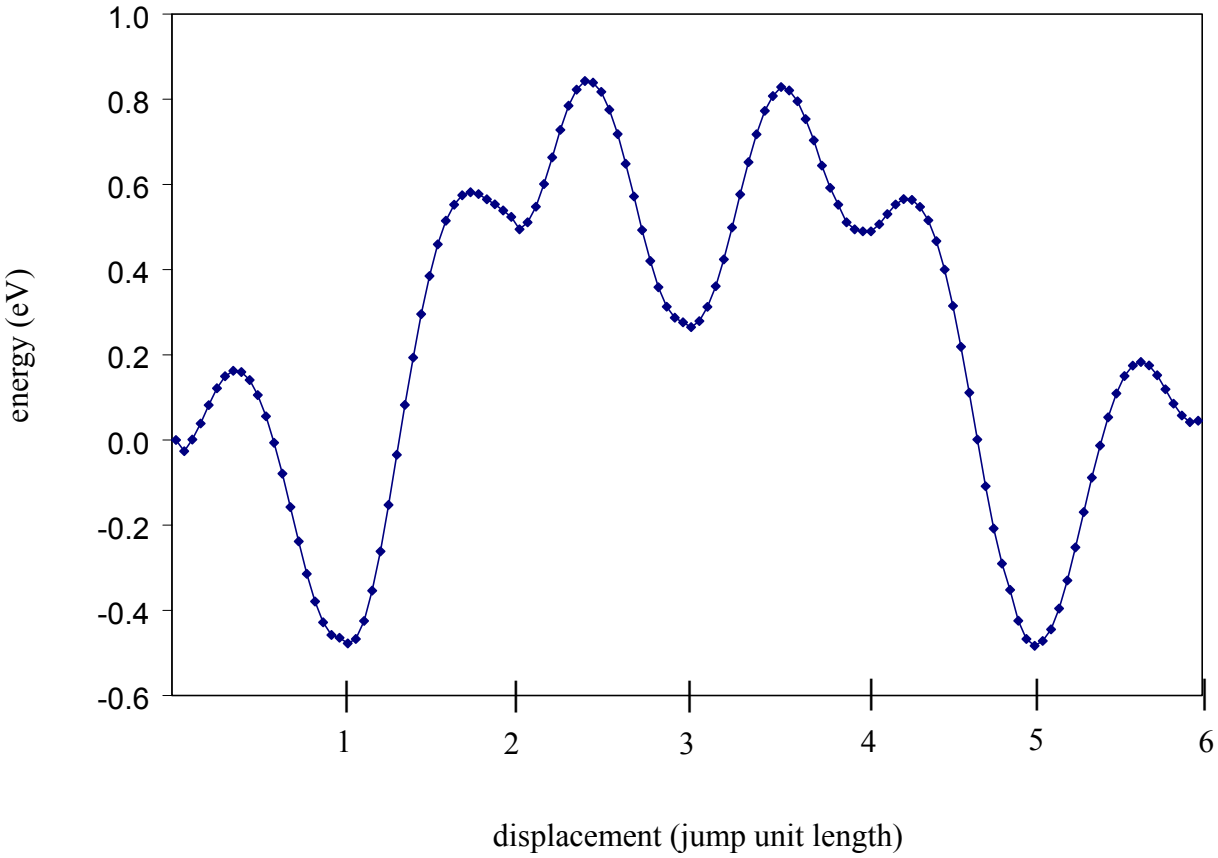

Figure 3.2: Energy-displacement curve for a [110] 6JPC in Al vacancy.

fig. 3.2) is E_{vAl}^{meff}=0.84 eV. From the energy-displacement curve (see fig 3.2) the energy value after jump 1, being negative, suggests that this configuration is expected to be more stable than the initial configuration. The values of highest migration energy found with this potential are much lower than the values of E_{vAl}^{m}=2.42 eV and E_{vNi}^{m}=2.44 eV, that were calculated with the same method by Mishin and Farkas [4]. The difference of the results between these two investigations stresses the influence of the potentials in this type of calculation. The activation energies of the 6JPC are Q_{Ni}^{6JPC}= 2.02 eV for a Ni vacancy mechanism and Q_{Al}^{6JPC}= 2.07 eV for an Al vacancy mechanism. For a diffusion occurring via 6-jump cycle, both the Al vacancy mechanism and the Ni vacancy mechanism are expected to have about the same contribution in a stoichiometric NiAl.

Based on the activation energy values calculated by molecular statics, the diffusion is expected to occur via 6-jump cycle in a Ni and Al vacancy mechanism. For diffusion of both point defects, the values of the activation energy are about 1eV lower for a 6JPC mechanism than for a NNN mechanism. Once again, it is important to stress that this conclusion and the actual numbers are strongly dependent on the potential used.

3.2 Molecular Dynamics Investigation

Molecular dynamics simulations are performed for both cases: a Ni vacancy migration and an Al vacancy migration. Two series of statistics are obtained. The different mechanisms involved in the vacancy migration are reported following a given procedure and analyzed in detail.

3.2.1 Computational Procedure

All the statistical analysis reported below is based on simulations using a standard molecular dynamics simulations code using a constant temperature algorithm. We used a block that is cubic in shape with repeating periodic boundary conditions in the three directions. This means that when the vacancy jumps to a site outside the block it is reintroduced in the other side of the block.

Our simulation size was of 125 unit cells arranged in a cube with dimension 5a×5a×5a, as illustrated in Figure 3.3. The vacancy is initially introduced in either a Ni-type site or in an Al-type site. The block has 249 atoms that are arranged in a perfectly ordered structure.

The atomic interaction is described by the EAM potentials [42]. The lattice parameter used is that of equilibrium at the temperature of the simulations. The potentials predict that the perfect stoichiometric equilibrium lattice parameters at 1100 K (827°C), 1150K (877°C), and 1200K (927°C), are respectively a_{1100}=2.9303 Å, a_{1150} = 2.9335 Å, and a_{1200}=2.9363 Å. These values are, as expected, larger than 0K lattice parameter a_0 which is 2.8756 Å.

The simulations are performed at three different temperatures: 1150K and 1200K for the Al rich compound, and 1100K and 1150K for the Ni rich compound. This choice has been motivated by the fact that these temperatures are low enough to keep a high degree of order and high enough to allow the observation of a statistically meaningful number of diffusion events in reasonable computing time. Our goal is to be able to follow in detail about one hundred different diffusion events. It is important that order would be maintained at the temperature of study in order to insure that we are not studying a transient type of regime.

The diffusion processes are studied over a range of 1,250,000 iterations at 1150K and 750,000 iterations at 1200K in the case of an Al rich compound, and 1,250,000 iterations at 1100K and 750,000 iterations at 1150K in the case of a Ni rich compound. We used a time step of $2x10^{-3}$ nanoseconds, meaning that this corresponds to study the diffusion phenomena during 2.5 ns for 1150 K and 1.5 ns for 1200K for the Al rich compound. The same simulation times, 2.5 ns at 1100 K and 1.5 ns at 1150K, were applied for the Ni rich compound.

The details of the diffusion process are studied by monitoring the atom displacements every 50000 steps (0.1 ns). This allows the identification of the initiation of diffusion cycles. The atomic displacements are then monitored every 50 to 100 steps or 0.1 to 0.2 ps in order to study the detailed mechanism and associate the detailed sequencing of events within a particular cycle.

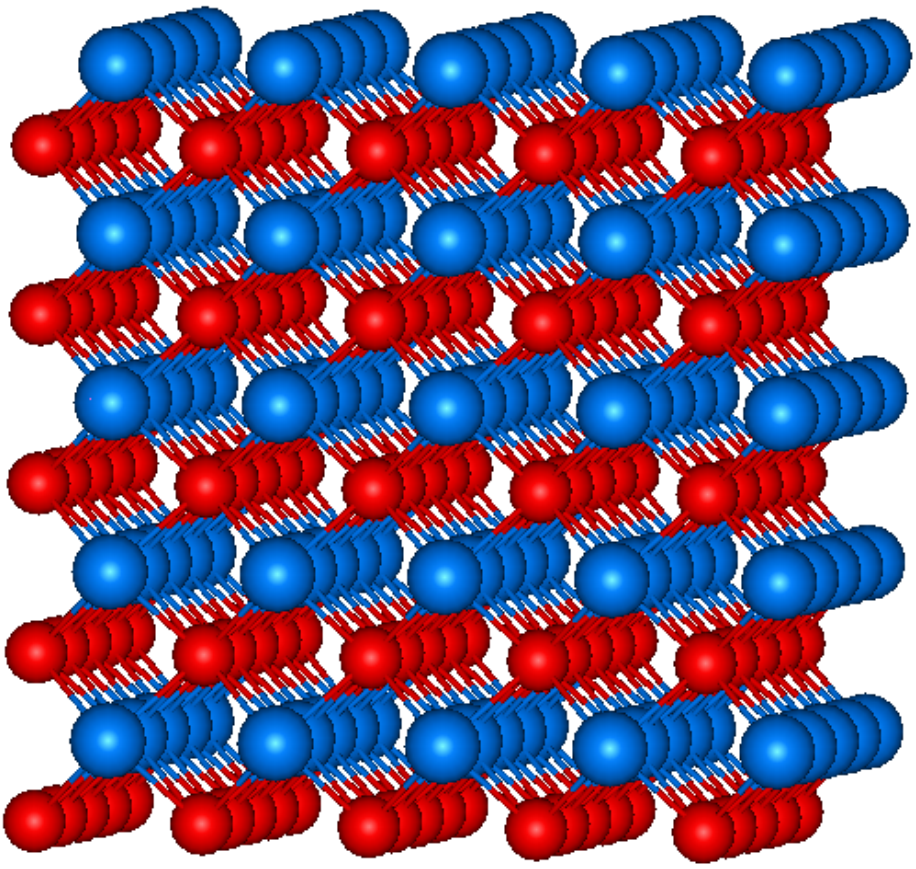

Figure 3.3: Graphical representation of the NiAl simulation block.

3.2.2 Statistical Procedure

For a statistical analysis of the results we classify the diffusion event data according to the different mechanisms they refer to. A diffusion event is taken to be one or more atomic jumps from initiation to the restoration of the perfect order of the lattice. The different types of events reported are: the 6 jump cycles, 10 jump cycles, 14 jump cycles, and failed attempts with the vacancy returning to the original position. Thus in the case of a starting Ni vacancy a total of 93 events were studied. A total of 120 events were studied in the case of a starting Al vacancy.

The 6JPC are the most common successful diffusion event. We consider the frequency of the different possible types of cycles. We also differentiate the uninterrupted 6JPC (see fig. 1.3) from the interrupted ones, where a neutral atom (not involved in the resulting 6JPC) jumps to the vacant site and goes back to its previous configuration within the sequence. We differentiate the three different types of 6JPC (see fig. 1.4): the [110] cycle, the [100] straight cycle and the [100] bent cycle. Almost all the cycles observed are [110] cycles.

The 10JPC is a new mechanism observed in the present investigation, in which the vacancy follows a definite path of 10 jumps. A complete analysis of the mechanism is reported below. As in the 6JPC case, we differentiate the uninterrupted 10-jump cycles (see fig. 3.11) from the interrupted ones. The way of defining them is exactly the same as for the 6JPC. This new mechanism occurs with less frequency than the 6JPC but it still may be significant to the overall diffusion process.

The 14JPC is also a new mechanism and in this case, the vacancy follows a definite path of 14 jumps. This mechanism is not as common.

The category of failed attempts returning to the original position of the vacancy corresponds to the events where one or several atoms jump in a nearest neighbor site and go back to their original positions. We report the different situations: the first being

where one atom jumps and goes back. In the second type two atoms jump one after another and go back in the opposite order (the second atom goes back and then the first one), and finally the case where more than two atoms jump and go back in successive steps reversing the order of the initial attempt.

We also had a few cases of undefined uncompleted cyclic mechanisms. These are not common, and may be the indication of the fact that thermodynamically, a small degree of disorder is expected since the order parameter at these temperatures is close to but not exactly one.

3.2.3 Diffusion of the Ni Vacancy

The results of the simulations for a Ni vacancy are presented in Table 3.2 and Table 3.3. A total of 26 events are observed at 1150 K and 67 events at 1200K. The total number of runs performed at each temperature corresponds to study of diffusion during 30 ns at 1150 K and 34.5 ns at 1200 K.

There are two main types of events occurring during the simulation process. The first one is, as expected, the jump cycle. Most of these are 6 jump cycles but there are also 10 and 14 jump cycles. These events represent about half of the total events studied. The second main type of event is the failed attempt for a cycle, which is reversed to the original configuration.

The 6 jump cycles are the primary mechanism involved in the diffusion. These account for about 40% of the total events observed. Some of the 6 jump cycles are interrupted by the inclusion of an extra jump at some point within the cycle. These interrupted 6 jump cycles correspond to 11% of all the 6jump cycles.

Table 3.2: Statistical occurrence of the various events observed for a Ni vacancy during 30 ns at 1150K (15 million time steps).

Events	Specifications	Values	Total
6-jump cycles	Uninterrupted	42.3%	
	Interrupted	0%	
	[110] cycles	78%	
	[100] straight cycles	0%	
	[100] bent cycles	12%	42.3%
10-jump cycles	Uninterrupted	3.8%	
	Interrupted	3.8%	7.6%
14-jump cycles		0%	0%
Attempt returning to the original position	Involving 1 atom	19%	
	Involving 2 atoms	15.4%	
	Involving more than 2 atoms	4%	38.6%
Other		11.5%	11.5%
		Total	100%

Table 3.3: Statistical occurrence of the various events observed for a Ni vacancy during 34.5 ns at 1200K (17.25 million time steps).

Events	Specifications	Values	Total
6-jump cycles	Uninterrupted	32.8%	
	Interrupted	7.4%	
	[110] cycles	100%	
	[100] straight cycles	0%	
	[100] bent cycles	0.0%	40.2%
10-jump cycles	Uninterrupted	4.4%	
	Interrupted	1.5%	5.9%
14-jump cycles		1.5%	1.5%
Attempt returning to the original position	Involving 1 atom	6%	
	Involving 2 atoms	26.9%	
	Involving more than 2 atoms	6%	38.9%
Other		13.5%	13.5%
		Total	100%

Differentiating the different types of 6JPC, we can report they mainly are [110] cycles. Thus at 1200K we have 100% of [110]-6JPC and 78% at 1150K. The other type of 6JPC occurring with a low probability is only the [100] bent cycle. These results are in conflict with the theoretical model proposed by Arita et al. [10], but agree with the reports of most studies that estimate the [110] cycle to be the most probable one. Experimental studies on the Fe diffusion in a B2-FeAl [12,13] showed the diffusion occurs mostly in a [110]-jump cycle type, but with a probability $P_{110}=1.9\pm0.1\times P_{100}$ that is much lower than that found in the present study.

The 10 jump cycles respectively correspond to about 6-7% of the events. These include the regular and the interrupted 10 jump cycles. The statistical occurrence of these events is quite similar at both temperatures and much lower than that corresponding to the 6-jump cycle.

The 14-jump cycle, corresponding to 0% of the events at 1150 K and 1.5% at 1200 K, is a rare event.

The failed cycle attempts account for 38.6% of the events at 1150K and 38.9% at 1200K. At 1150K, most of these are cycle attempts that reversed after the first jump. This can be understood on the basis of the potential energy curve in figure 3.1. After the first jump, the system is in a local valley with a relatively high energy and it is reasonable that the system tends to go back to its original configuration rather than getting over the second energy barrier of 1.28 eV. If the system has enough energy to accomplish both jumps 1 and 2 it is then in a local valley. Again, it is reasonable that, after jump 2, the system has a high probability of going back to its original position because the energy barrier of jump 3 is higher than that needed for reversing jump 2. At 1200 K, most of the cycles are reversed after jump 2 with 26.9% of the total event.

Finally, in observing the numbers related to the category other, where the final configuration of the run is complex and temporary disordered, we can observe they represent the less probable event with 11.5% of the total events at 1150 K, and 13.5% at

1200 K. These complex diffusion paths can be interpreted as resulting from the small deviation of perfect order, which already occurs at this temperature.

In the case of a Ni vacancy, according to the activation energy values (see table 3.1 and fig. 3.1), the 6JPC is expected to be more favorable than the next nearest neighbor mechanism. In agreement with this expectation, the latter mechanism was not observed in our simulations. At both temperatures studied, the 6-jump cycle is the main diffusion mechanism.

3.2.4 Diffusion of the Al Vacancy

The results of the simulations for an Al vacancy are presented in Table 3.4 and Table 3.5. A total of 76 events are observed at 1100 K and 44 events at 1150 K. The diffusion is studied during 27.5 ns at 1100 K and 15 ns at 1150 K.

The most common event is a failed cycle attempt that is reversed after the first jump. The high probability of this event can be understood on the basis of the potential energy (see fig. 3.2) curves where the highest energy barrier occurs after the first jump, making it much more probable for the vacancy to return to its original position than to proceed further in the cycle.

Besides the failed cycle attempt, the most probable event is again the six-jump cycle. They are all of a [110]-type and represent 22.4% of the total events at 1100 K and 13.5% at 1150 K. The interrupted cycles correspond to about 6% of the 6JPC at 1100K and 50% at 1150 K.

In the case of the Al vacancy diffusion, we also report an extra type of 6JPC where the Al vacancy first jumps to a Ni site, and where the diffusion then proceeds through a Ni vacancy type 6-jump cycle. This mechanism can be expected to occur based on the migration energy curves predicted by the interatomic potential used (see fig. 3.2). Indeed, after jump 1, the system is in a low energy configuration that is similar to

Table 3.4: Statistical occurrence of the various events observed for a Al vacancy during 27.5 ns at 1100K (13.75 million time steps).

Events	Specifications	Values	Total
6-jump cycles	Uninterrupted	11.9%	
	Interrupted	0%	
	[110] cycles	100%	
	[100] straight cycles	0%	
	[100] bent cycles	0%	11.9%
6-jump cycles-Ni vacancy type	Uninterrupted	9.2%	
	Interrupted	1.3%	
	[110] cycles	100%	
	[100] straight cycles	0%	
	[100] bent cycles	0%	10.5%
10-jump cycles	Uninterrupted	1.3%	
	Interrupted	0%	1.3%
Attempt returning to the original position	Involving 1 atom	57.9%	
	Involving 2 atoms	7.9%	
	Involving more than 2 atoms	6.6%	72.4%
Other		3.9%	3.9%
		Total	100%

Table 3.5: Statistical occurrence of the various events observed for an Al vacancy during 15 ns at 1150K (7.5 million time steps).

Events	Specifications	Values	Total
6-jump cycles	Uninterrupted	2.3%	
	Interrupted	6.7%	
	[110] cycles	100%	
	[100] straight cycles	0%	
	[100] bent cycles	0%	9%
6-jump cycles-Ni vacancy type	Uninterrupted	4.5%	
	Interrupted	0%	
	[110] cycles	100%	
	[100] straight cycles	0%	
	[100] bent cycles	0%	4.5%
10-jump cycles	Uninterrupted	2.4%	
	Interrupted	0%	2.4%
Attempt returning to the original position	Involving 1 atom	61%	
	Involving 2 atoms	13.8%	
	Involving more than 2 atoms	2.4%	77.2%
Other		6.9%	6.9%
		Total	100%

the initial state of a Ni vacancy diffusion mechanism. This type of 6JPC accounts for 47% of the 6JPCs at 1100 K and 33% at 1150 K.

The occurrence of the 10JPC is rare at both temperatures: 1.3% at 1100K and 2.4% at 1150K. The contribution of this mechanism to the diffusion is much lower than that of the 6JPC. The 10JPC observed are all uninterrupted. No Ni vacancy type 10JPC is observed as in the case of the 6JPCs reported above. No 14-jump cycles are observed.

The failed cycle attempts are the most common event with 72.4% at 1100K and 77.2% at 1150K. Most of these cycle attempts are reversed after the first jump. This can be understood on the basis of the potential energy curve in figure 3.2. After jump 1, the system is a local valley, and the energy barrier of 1.05 eV required to accomplish jump 2 is considerably higher than the 0.63 eV required to reverse jump 1. The failed cycle attempt reversing after the second jump corresponds to the second most probable failed cycle with 7.9% at 1100 K and 13.8 % at 1150 K. This can be understood by referring to the potential energy curve where the energy barrier required to complete jump 3 is seen to be much higher than that to reverse jump 2.

The category other, which characterizes a small deviation of perfect order, accounts for 3.9% at 1100K and 6.9% at 1150K, and represents the less probable event.

In the case of Al vacancy diffusion, we can draw similar conclusions as in the case of the Ni vacancy. The only highlighted diffusion mechanisms are the jump cycle sequences (mainly the 6JPCs), and we do not observe any next nearest neighbor jumps, as expected from the statics activation energy calculations (see table 3.1 and fig. 3.2).

3.2.5 Detailed Sequential Analysis of the Ni Vacancy [110] Six Jump Cycles

The curves reported in figures 3.4-3.7 correspond to the displacements of the three jumping atoms involved in four different [110] 6JPC sequences. The displacements

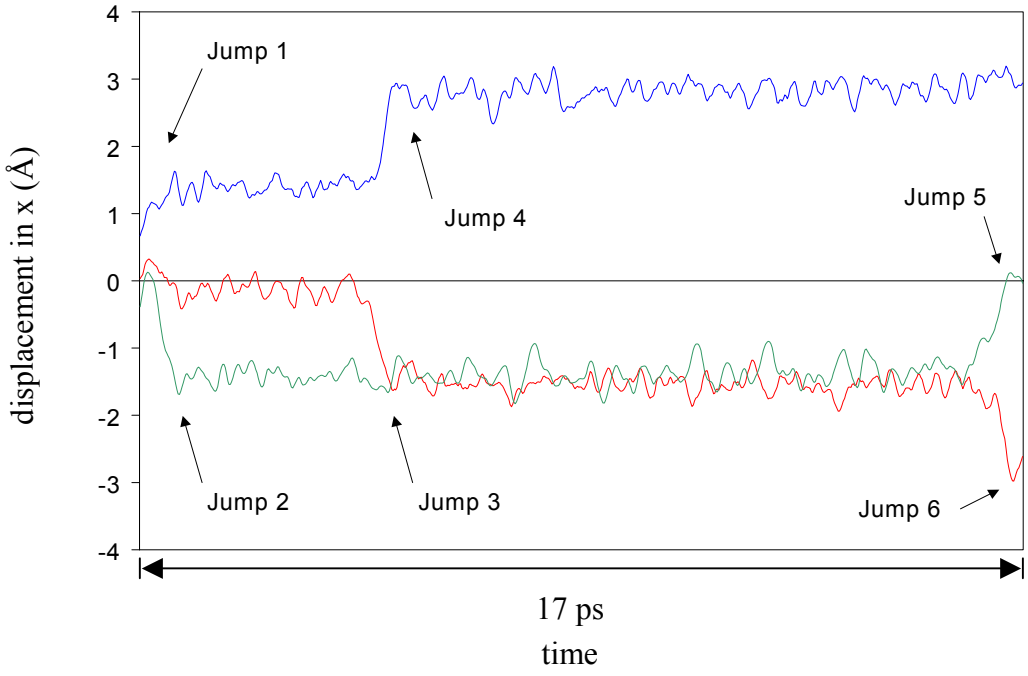

Figure 3.4: Displacement versus time curve of a [110] jump cycle of Ni-vacancy type.

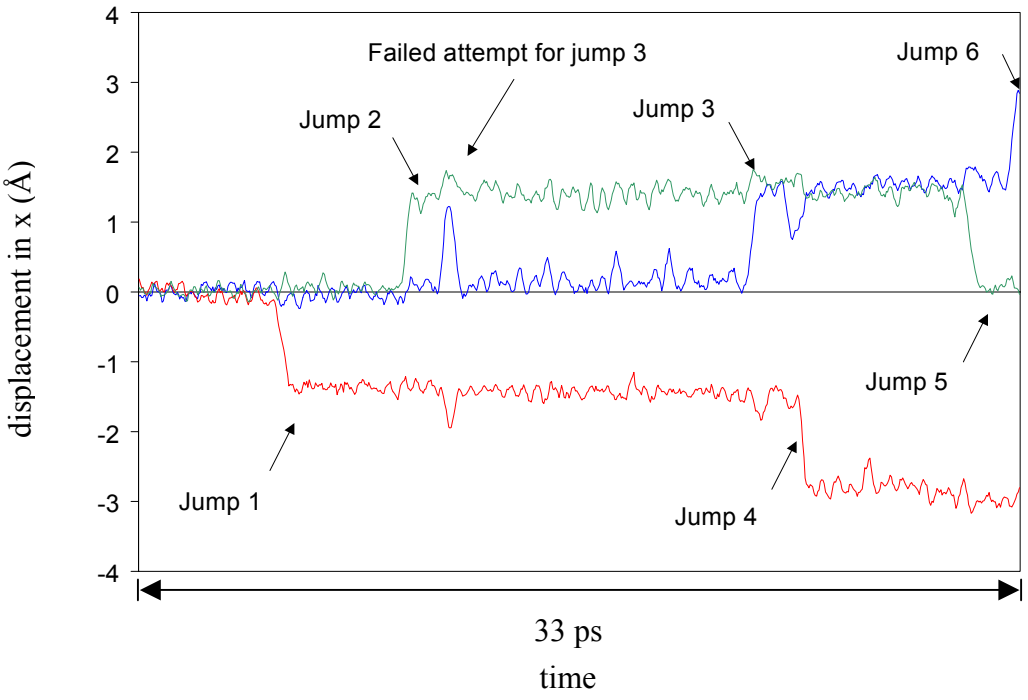

Figure 3.5: Displacement versus time curve of a [110] jump cycle of Ni-vacancy type

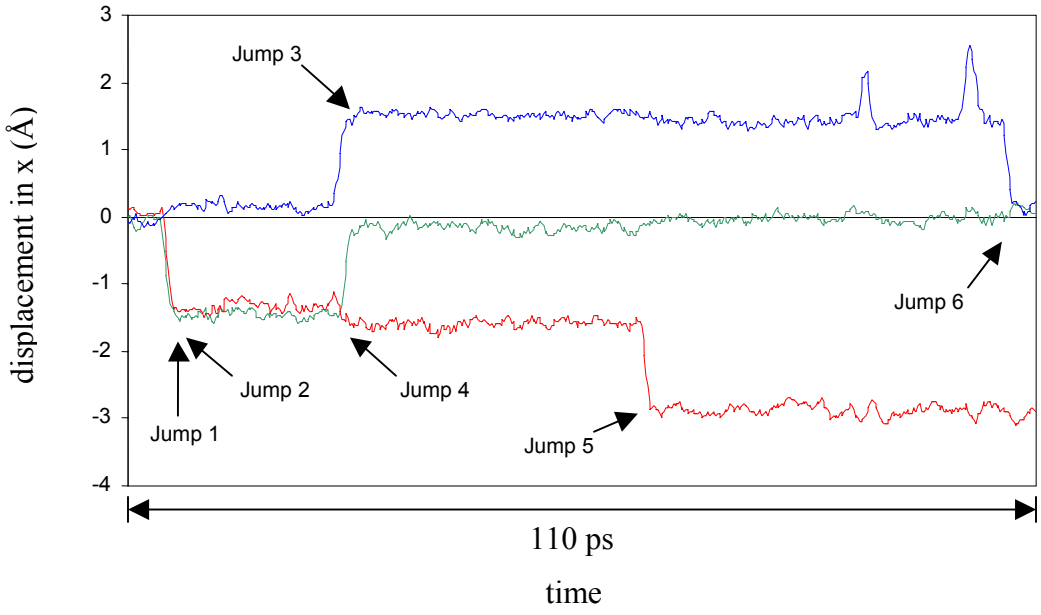

Figure 3.6: Displacement versus time curve of a [110] jump cycle of Ni-vacancy type.

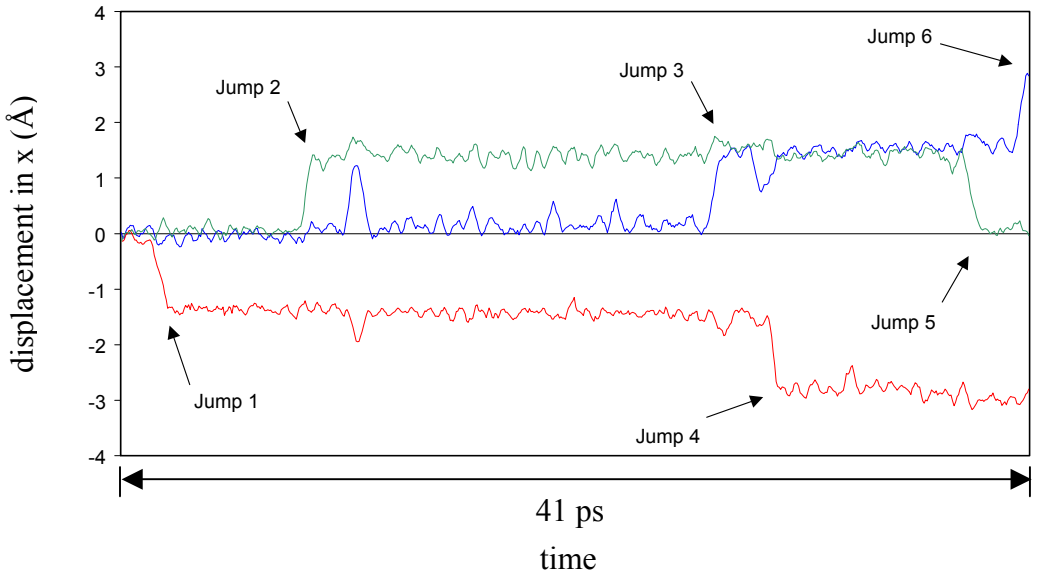

Figure 3.7: Displacement versus time curve of a [110] jump cycle of Ni-vacancy type.

are reported along the x direction as a function of time. In a 6JPC mechanism, the atomic migrations are coordinated in the three directions and it is only necessary to report one direction to determine when the jump occurs. The 6JPC sequences reported in figures 3.4, 3.5 and 3.7 occur at 1200 K, and the sequence reported in figure 3.6 at 1150 K.

The total time that it takes to complete a cycle varies from 15 to 45 ps for the 6JPCs at 1200 K, and is about 110 ps for the sequence at 1150 K.

The different curves suggest that, within the sequence, some specific jumps are correlated. In the first sequence reported in figure 3.4, jumps 1-2, 3-4, and 5-6 clearly occur together and can be seen as coordinated. In the second sequence (see fig. 3.5), we again have coordinated jumps. Jumps 1-2 appear clearly coordinated. Then there is a failed attempt for jump 3 by itself, followed by a failed attempt for jump 3-4 coordinated. Finally jumps 3-4 and 5-6 clearly occur together completing the sequence. In the third curve (see fig. 3.6), similarly to figures 3.4 and 3.5, jumps 1-2 and 3-4 occur together and are coordinated. However, the system completes jump 5 and stays in this configuration for a while (almost half of the time of the sequence) before completing the sequence. In the last curve reported in figure 3.7, the jumps seem to be coordinated but clearly do not occur simultaneously. Jumps 1-2 are completed in about 7 ps and the fact that they are coordinated is questionable. However, jumps 3-4 and 5-6 occurring in a much shorter time of 3 and 2.5 ps respectively can be seen as coordinated.

On the basis of the activation energy curve reported in figure 3.1, the fact of correlating jump 1-2, 3-4, and 5-6 (see figure 3.4 and 3.5), can be seen as a way of avoiding the high-activated states after jumps 1, 3, and 5.

3.2.6 Detailed Sequential Analysis of the Al Vacancy [110] Six Jump Cycles

Similarly to section 3.2.5, we obtain in figures 3.8, 3.9 and 3.10, curves describing the displacements along the x direction of the jumping atoms involved in three different [110] 6JPCs. Figure 3.8 and 3.9 represent two 6JPC sequences occurring at 1100 K, and figure 3.10 represents a sequence occurring at 1150 K.

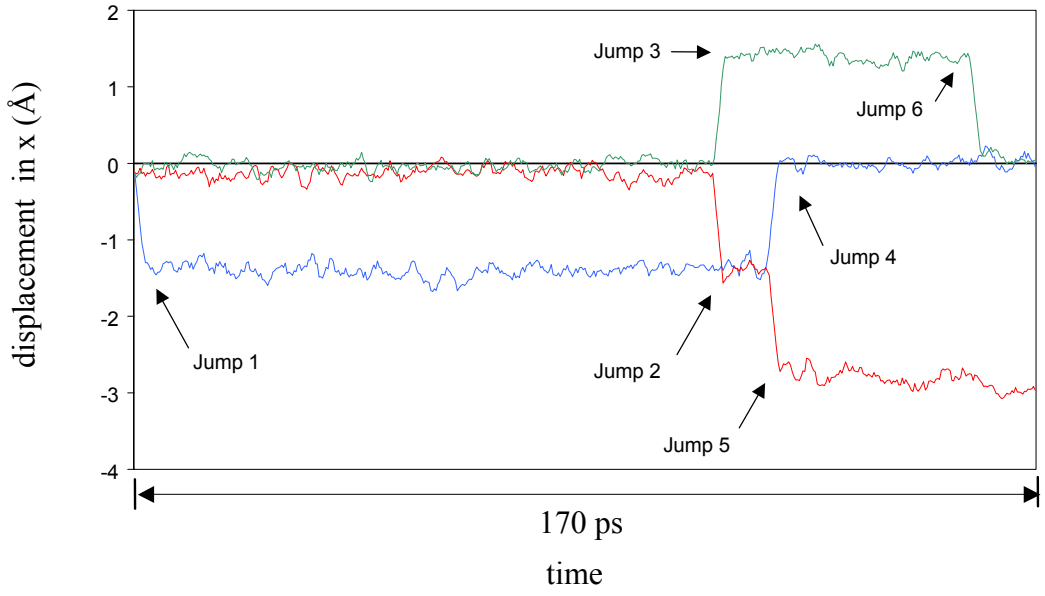

Figure 3.8: Displacement versus time curve of a [110] jump cycle of Al-vacancy type.

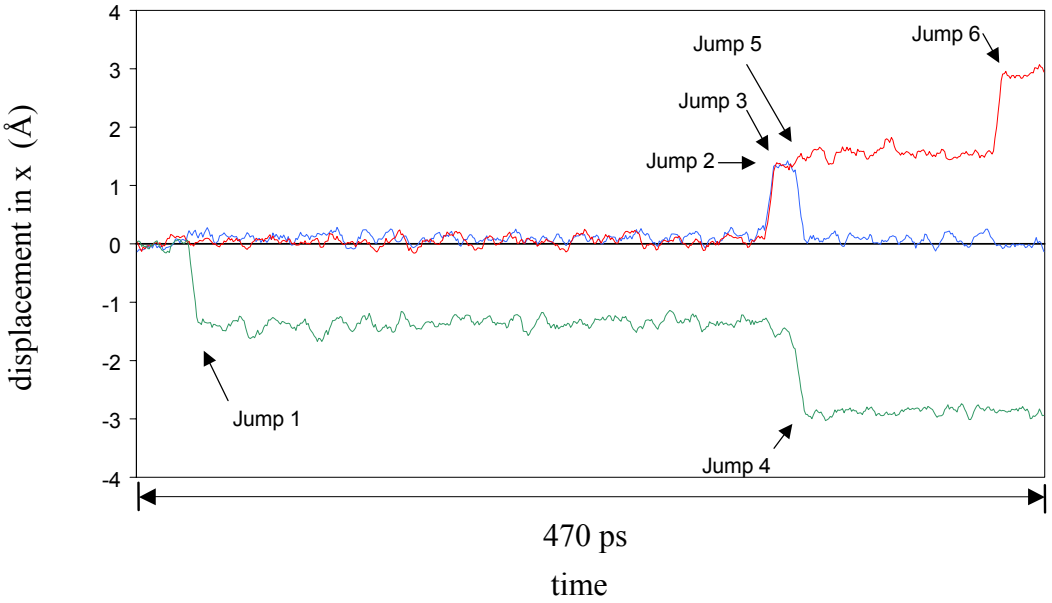

Figure 3.9: Displacement versus time curve of a [110] jump cycle of Al-vacancy type.

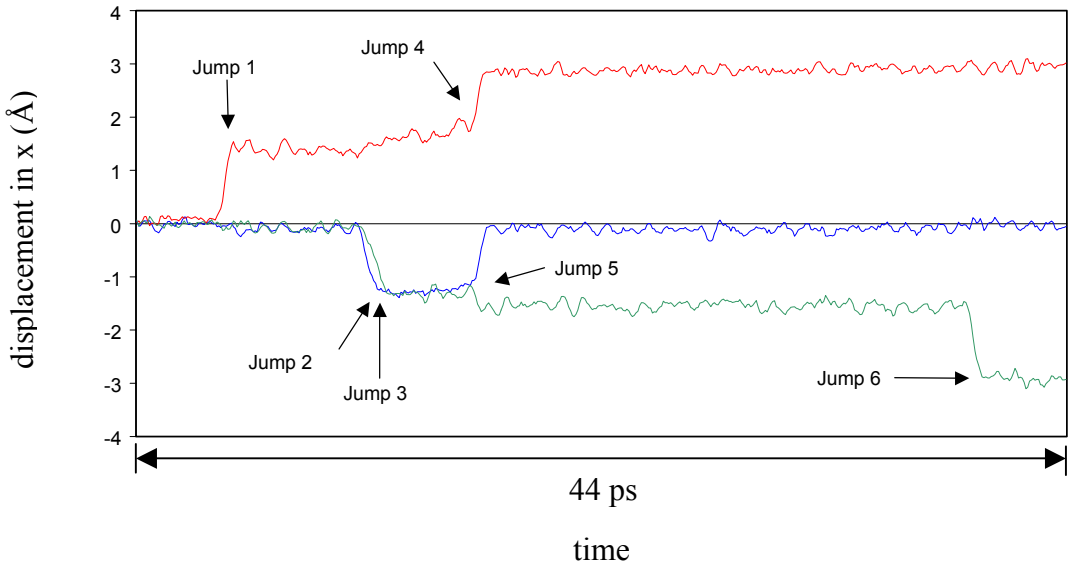

Figure 3.10: Displacement versus time curve of a [110] jump cycle of Al-vacancy type.

As observed in the case of a Ni vacancy, we obtain different time scales for the three reported 6-jump cycles. They vary from 170 ps to 470 ps for the sequences reported at 1100 K, is a much lower, 44 ps, at 1150 K.

In the present case, the behavior of the jumping atoms is less questionable than the other type of 6-jump cycle. In the three curves, jump 1 occurs by itself, then jumps 2-3 and 4-5 are correlated, and finally the jump 6 also occurs by itself. Similarly to the analysis done in the previous paragraph, we can suppose that the correlation of the jumps 2-3 and 4-5 has for effect to avoid the high activated state after jumps 2 and 4.

Considering the low values of the first energy barrier, Q_{Al}^{P1}, and the first local valley, Q_{Al}^{V1} (see potential energy curve in fig. 3.2), it is consistent that jump 1 occurs by itself, and that the system stays in this configuration for a while before jump 2 occurs. Regarding to the symmetry of the potential energy curve (see fig. 3.2), it is reasonable that a similar behavior is observed after jump 5.

3.3 New Cyclic Mechanisms Observed

The molecular dynamics investigation stresses the contribution of two new cyclic mechanisms to the diffusion process: the 10 and 14-jump cycles. These two mechanisms are seen to be less common than the 6JPC but have nonetheless an influence on the overall diffusion, especially the 10JPC. The two coming sections present an analysis of these mechanisms that is derived from the MD investigation described in section 3.2.

3.3.1 10-Jump Cycle Mechanism

The 10-jump cycle (10JPC) is a new mechanism involving five atoms wherein the vacancy migrates following a definite path of 10 jumps. The migration of the vacancy occurs via nearest neighbor sites destroying the partial order of the system. However, the order is recovered when the sequence is completed. In the following description we do not differentiate the 10JPC mechanisms by their vacancy migration type but by their geometrical characteristics.

A graphical analysis of the observed 10-jump cycle highlights two main types of mechanism. The first type of mechanism consists of a vacancy and five jumping atoms distributed in two parallel {110}-type planes. Two different types of initial configuration are observed for this (110) type 10JPC. The first initial configuration, 3/2, corresponds to a vacancy and three jumping atoms lying in the same {110} plane and two other atoms located in a plane parallel to the first one. The second initial configuration observed, 4/1, consists of a vacancy and four jumping atoms lying in the same {110} plane and one atom positioned above or below this plane. In this configuration, the vacancy migrates along a <111>-type vector and ends up in its original plane. For a 3/2 configuration, it migrates along a <110>-type vector and ends up in a parallel {110} plane. This 3/2 configuration 10JPC is the most common type of 10JPC, accounting for 67% of those observed. The (110) 10JPC with a 4/1 configuration is much less frequent and corresponds to 16% of the observed 10JPC. Figure 3.11 and 3.12 illustrate the Ni vacancy (110) 10JPCs with the two initial configurations 3/2 and 4/1 respectively. The second main type of 10-jump cycle consists of a vacancy and three jumping atoms lying in the same {100}-type plane and two other atoms within another plane perpendicular to the first one. The vacancy migrates along a <110>-type vector and ends up in the same plane as it was initially. This type of 10JPC is not very common with 17% of the observed 10JPC. Figure 3.13 illustrates a (100) 10JPC in the case of an Al vacancy mechanism.

The first five steps of both the (110) and (100) 10-jump cycles are identical to the first five steps of the 6-jump cycle they correspond to. For both initial configurations of (110) 10JPCs (see fig. 3.11 and 3.12), the first five atomic migrations occur within a same (110) plane as in a [110] 6JPC illustrated in figure 1.3. In a (100) 10JPC (see fig. 3.13), the first five steps correspond to the first five steps of a [100]-bent 6JPC (see fig. 1.4). The next step differs from classical 6-jump cycles because of the two extra atoms that accomplish their first nearest neighbor jumps as steps 6 and 7. The third atom is then completing its second nearest neighbor jump in step 5. Finally the fourth and fifth atoms

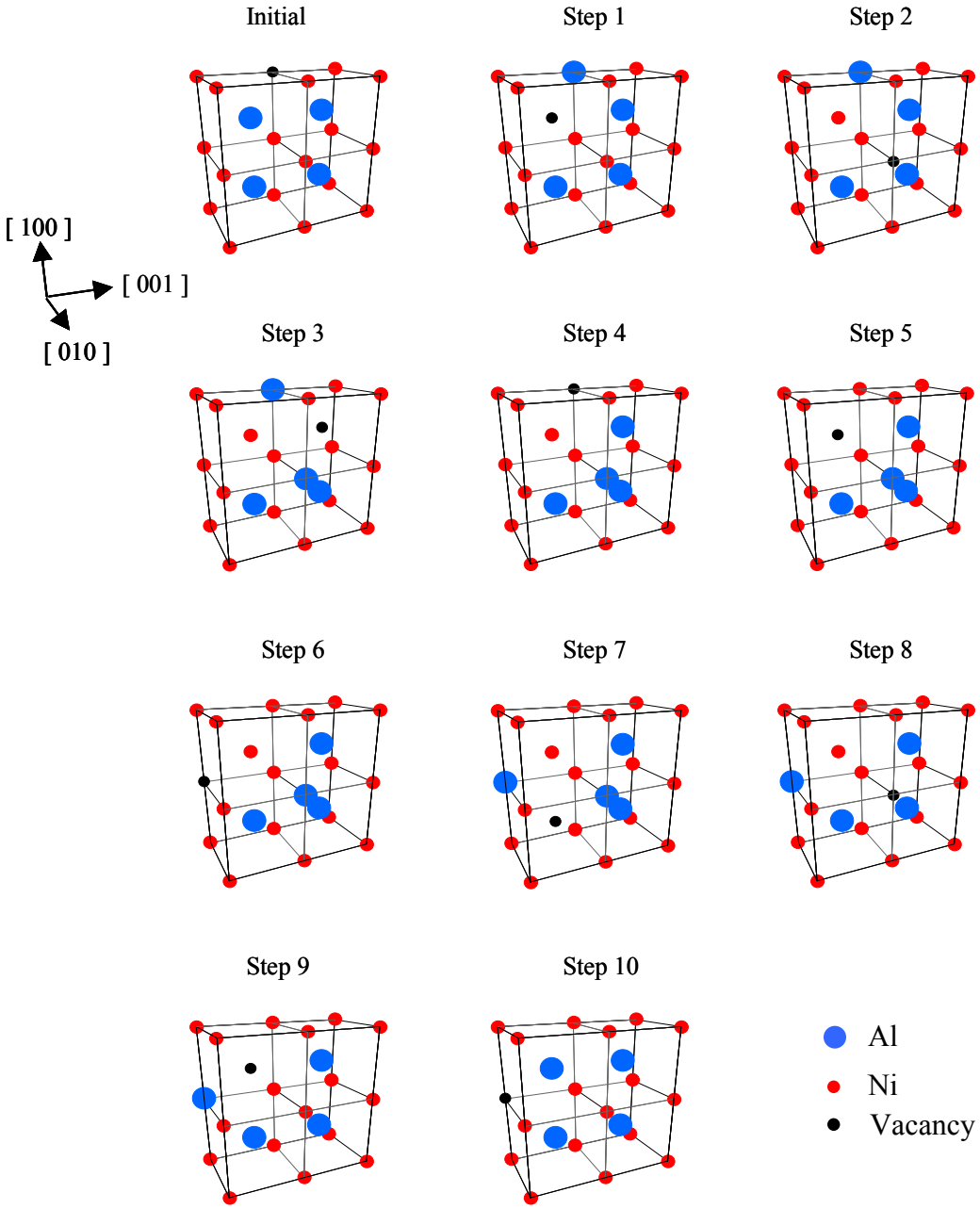

Figure 3.11: Graphical representation of a Ni vacancy (110)-type 10-jump cycle with a configuration 3/2 in NiAl.

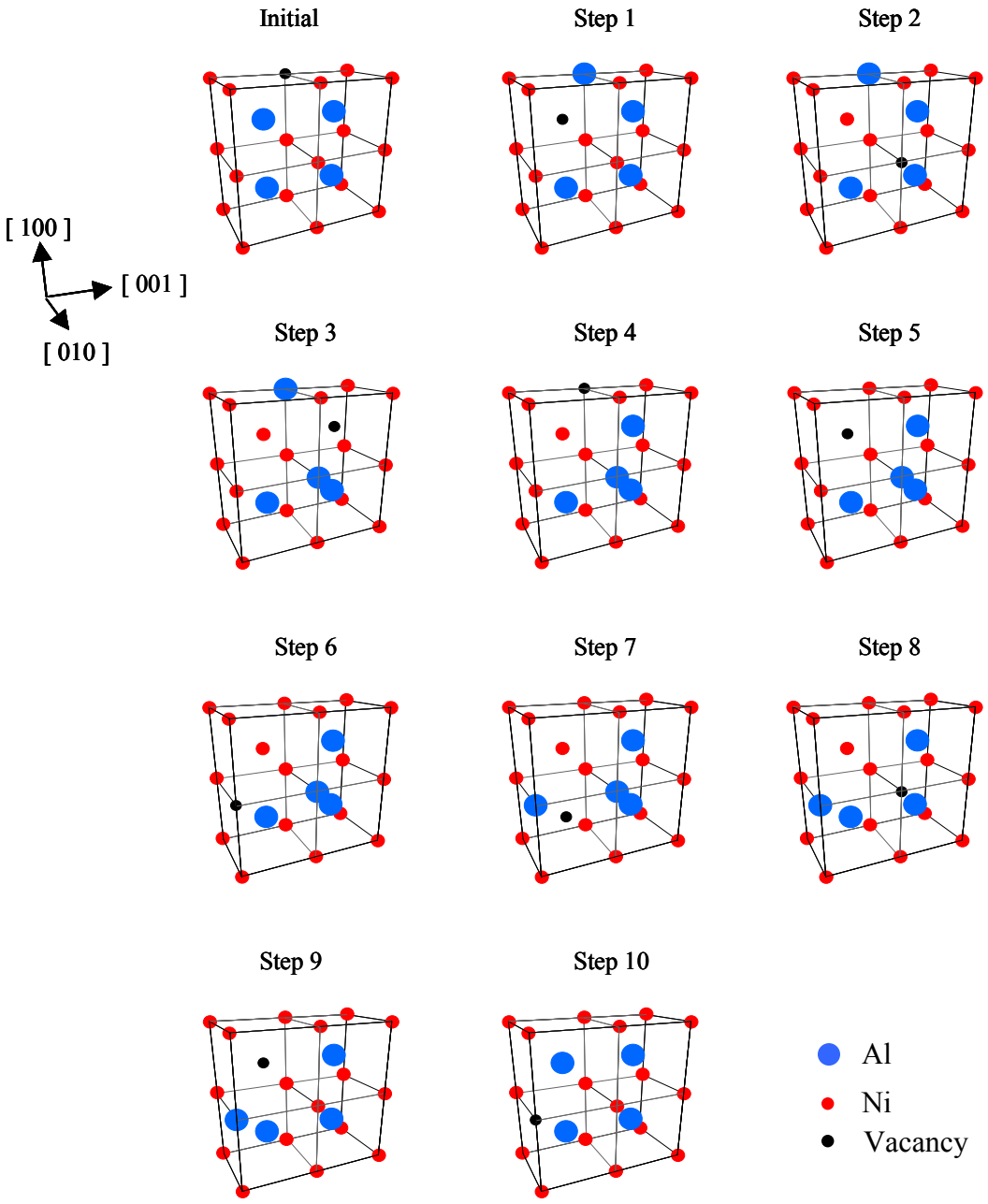

Figure 3.12: Graphical representation of a Ni vacancy (110)-type 10-jump cycle with a configuration 4/1 in NiAl.

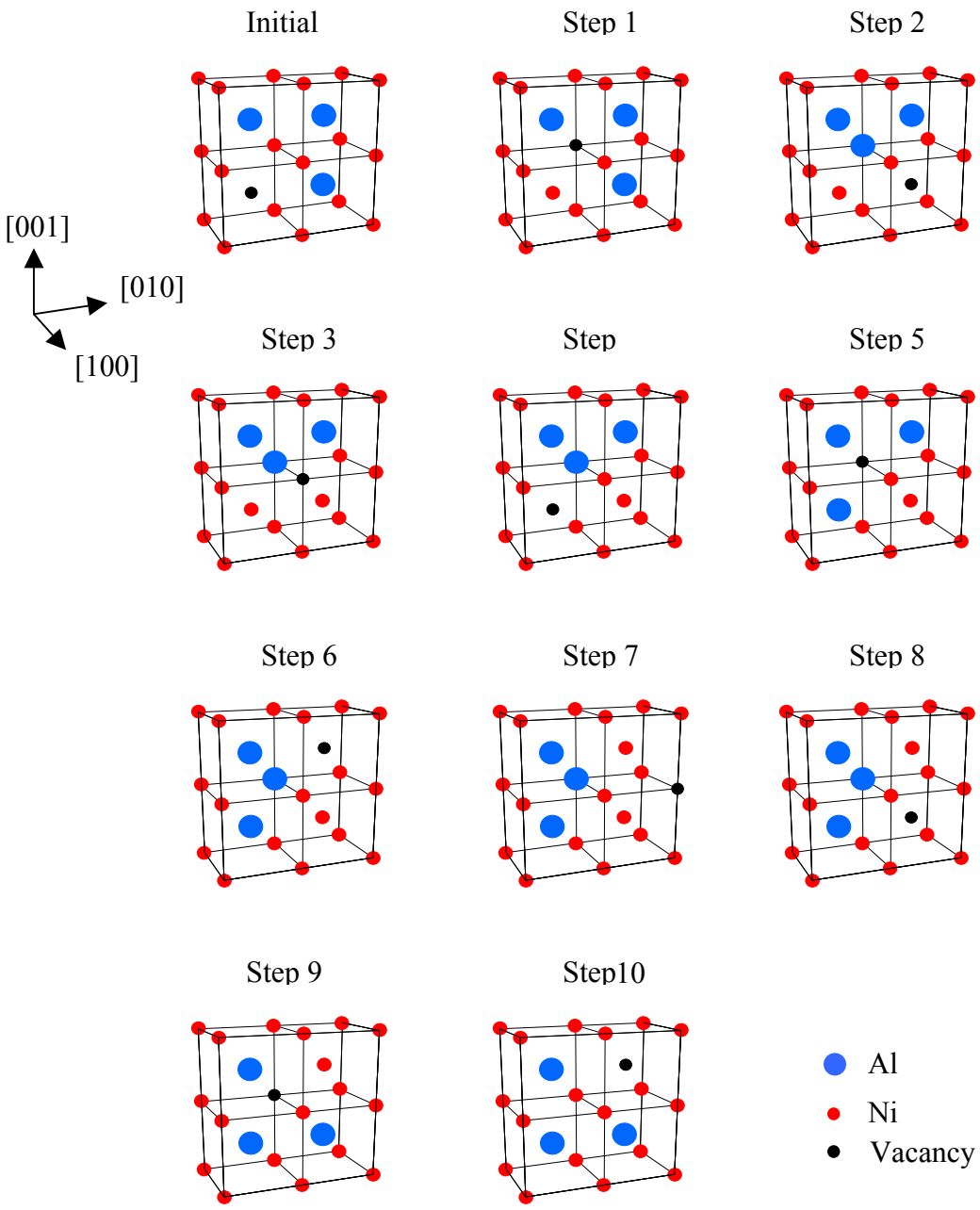

Figure 3.13: Graphical representation of an Al-vacancy (100)-type 10-jump cycle in NiAl.

complete the 10-jump sequence jumping back to their own sublattice. The order of the system is then recovered. For a 3/2 configuration (110) 10JPC, two atoms migrate in a first next nearest neighbor site and three migrate in a second next nearest neighbor site. For a 4/1 configuration (110) 10JPC, three atoms end up in a first next nearest neighbor site and two end up in a second next nearest neighbor site. Finally, for a (100) 10JPC, four atoms end up in a first next nearest neighbor site and the last one end up in second next nearest neighbor site.

From the geometrical analysis above, the 10-jump cycles are seen to be very similar to 6-jump cycles. However, the MD investigation reported in section 3.2 reveals that their contribution to the overall diffusion is much less important than that of the 6JPC. On the basis of geometric considerations, it is seen that the point defect configurations introducing the largest local disorder are identical for both 6JPC and 10JPC. As illustrated in figures 1.3, 3.11, and 3.12 for Ni vacancy mechanisms, the most unfavorable configuration: $2Al_{Ni}+Ni_{Al}+V_{Al}$ (see step 3, 5, 7) is identical for the 6 and 10-jumps cycles. From the migration energy curve in figure 3.1, this configuration corresponds to the highest activated state for the 6JPC. This geometric consideration may suggest that the two cyclic mechanisms have the same highest activated state, and that the difference in their diffusivity may be due to higher energy barriers or higher correlation factors in the case of a 10-jump cycle mechanism.

3.3.2 14-Jump Cycle Mechanism

The 14-jump cycle (14JPC) is a new mechanism involving seven atoms wherein the vacancy migrates following a definite path of 14 jumps. Similarly to the 6 and 10-jump cycles, the migration of the vacancy occurs via nearest neighbor sites destroying temporarily the partial order of the system. This mechanism is very rare and has only been observed in the case of a Ni-vacancy migration at 1200 K. The coming analysis cannot be generalized to all the 14-jump cycle mechanisms and corresponds to a description of the mechanism observed in the MD analysis reported in section 3.2.3.

As illustrated in figure 3.13, the 14JPC consists of a vacancy and six jumping atoms lying in the same {110}-type plane with an extra atom located below or above this plane. The vacancy migrates along a <100>-type vector and ends up in the same plane as it was originally.

The first 9 steps of the 14JPC are identical to the first 9 steps of a (110)-type 10JPC with a 4/1 configuration, as illustrated in figure 3.12 and 3.14. Steps 10 and 11 correspond to the first nearest neighbor jumps of the two extra atoms involved. The fifth atom completes its second nearest neighbor jump going back in its own sublattice (see step 12 in fig. 3.14). Finally, the two extra atoms achieve the 14-jump sequence recovering the perfect order of the crystal. Three atoms migrate in a first next nearest neighbor site and four migrate in a second next nearest neighbor site.

The investigation of the intermediate point defect configurations shows that the configuration introducing the largest local distortion is: $2Al_{Ni}+Ni_{Al}+V_{Al}$ (see steps 3, 7 and 11 in fig. 3.14). This configuration is again identical to the most unfavorable configuration in a 6-jump cycle. On the basis of this geometric consideration, identical conclusions as in the case of the 10JPC may be drawn. The highest activated states of the 6 and 14-jump cycles may be identical, and that the difference of diffusivity of these two mechanisms may be due to a higher energy barrier or a higher correlation factor for the 10-jump cycle mechanism.

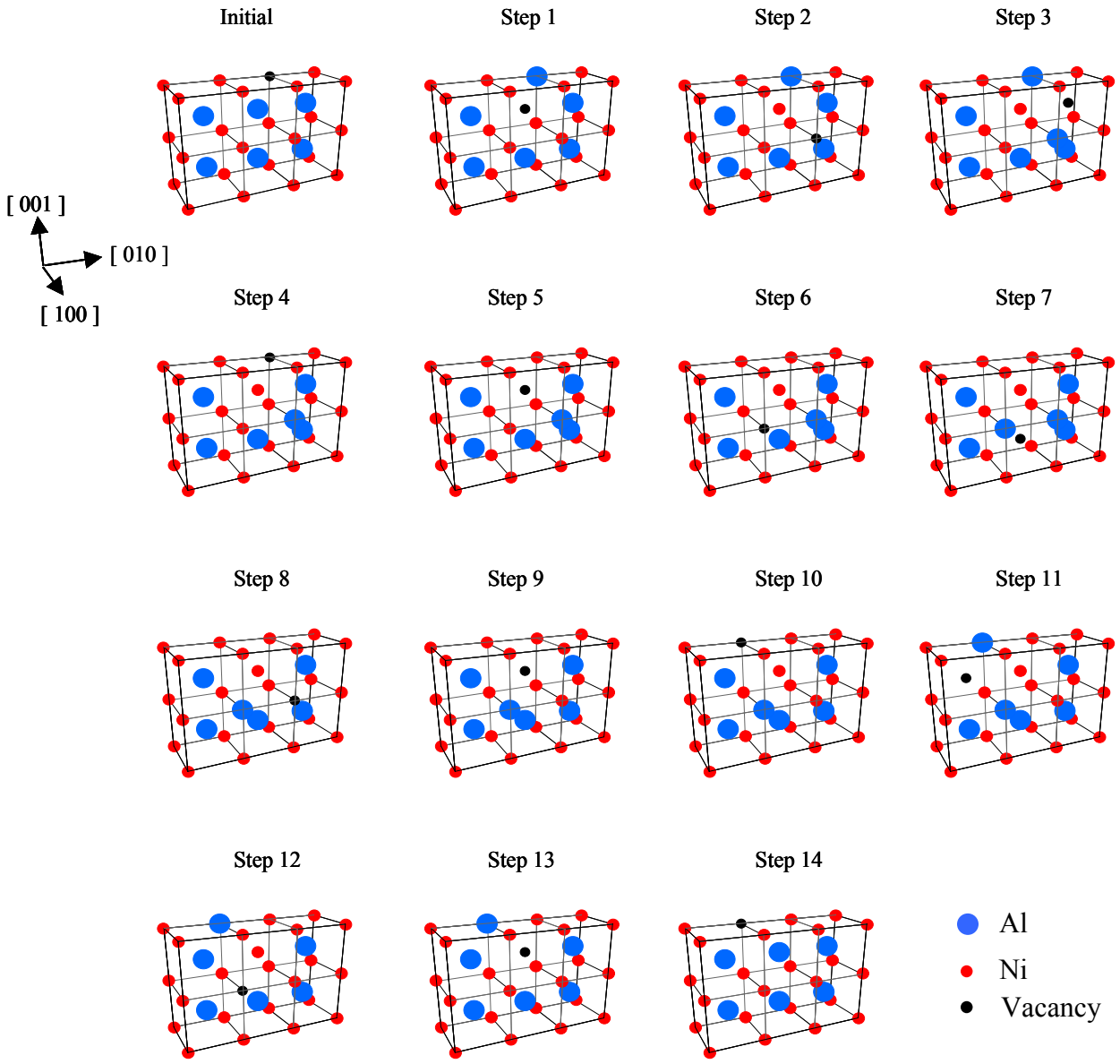

Figure 3.14: Graphical representation of a (110)-type 14-jump cycle in NiAl.

Chapter 4
GRAIN BOUNDARY DIFFUSION

4.1 Construction of the Grain Boundary

The Σ5(210)[001] grain boundary, which is investigated in this study, is first geometrically constructed by basic symmetry operations, and then relaxed via an energy minimization technique. Through this process, the lowest energy configuration of the grain boundary structure is found.

Initially, two distinct grains are aligned by a common (210) plane, as illustrated in figure 4.1. A 180° rotation about a $[\bar{1}\,2\,0]$ direction is applied to one of the grain relative to the other. This construction generates a coincident site lattice (CSL) grain boundary with a reciprocal density $\Sigma = 5$, where the two grains are tilted about the [001] direction by an angle, $\theta = 36.9°$ (see fig. 4.2).

The upper grain, 1, is then translated rigidly relative to the lower grain, 2, by a vector $t <t_x, t_y, 0>$ parallel to the grain boundary plane (see fig. 4.3). The CSL grain boundary is temporally destroyed by this translation such that it can be restored latter in a more stable structure through a relaxation process. A molecular statics method is applied to the simulation block illustrated in figure 4.3, to determine the relaxed structure. Atoms within the upper part of grain 1 and lower part of grain 2 (see fig. 4.3) are fixed in x and y directions, parallel to the grain boundary, and allowed to move in z direction, normal to the GB plane. Atoms sandwiched between the two slabs of fixed atoms are free. Periodic boundary conditions are applied in x and y, whereas they are fixed in the z direction. The relaxation of the translated structure is then performed by minimizing the total energy. Using a conjugate gradient method, the lowest energy structure is found with respect to the local atomic displacements. Figure 4.4 illustrates the lowest energy structure for the Σ5(210)[100] grain boundary found using this method.

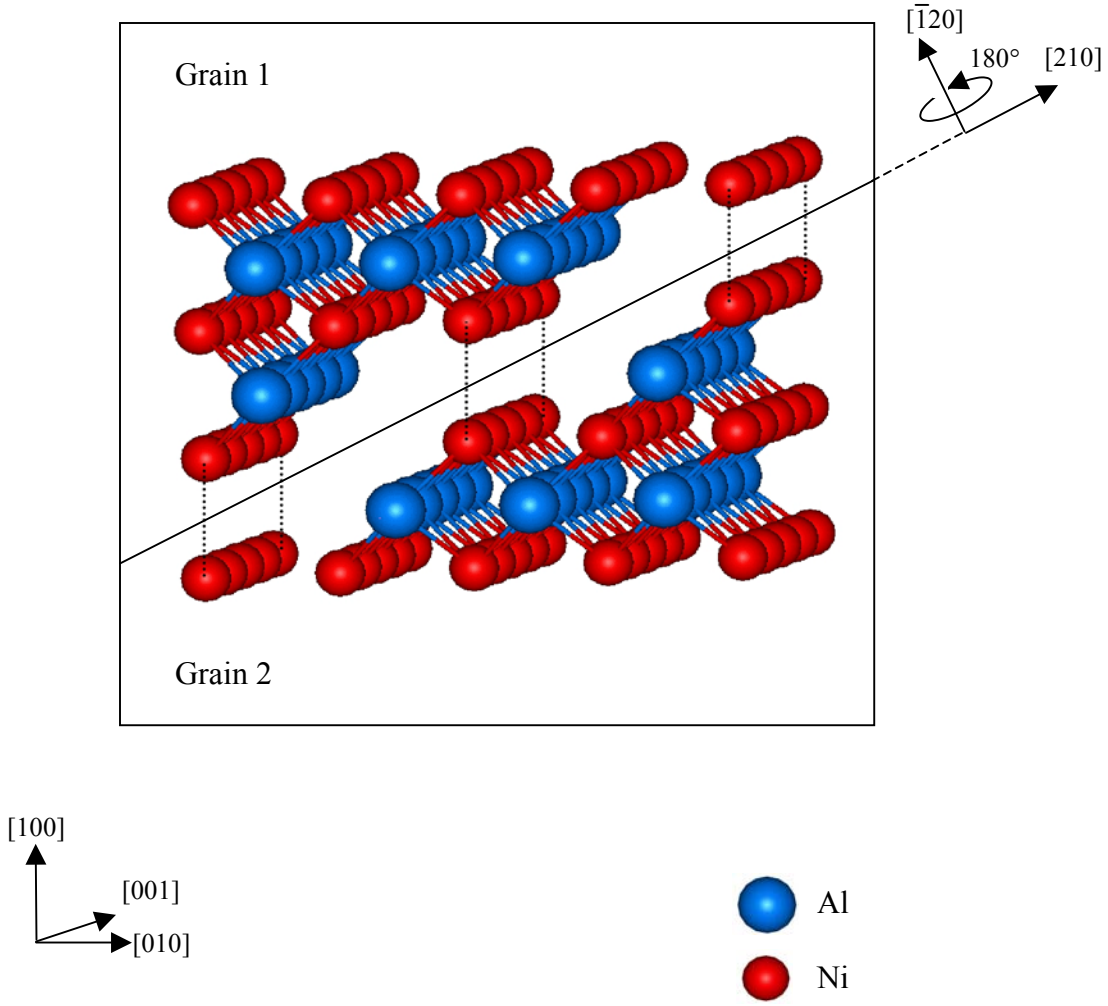

Figure 4.1: Initial configuration of grains 1 and 2.

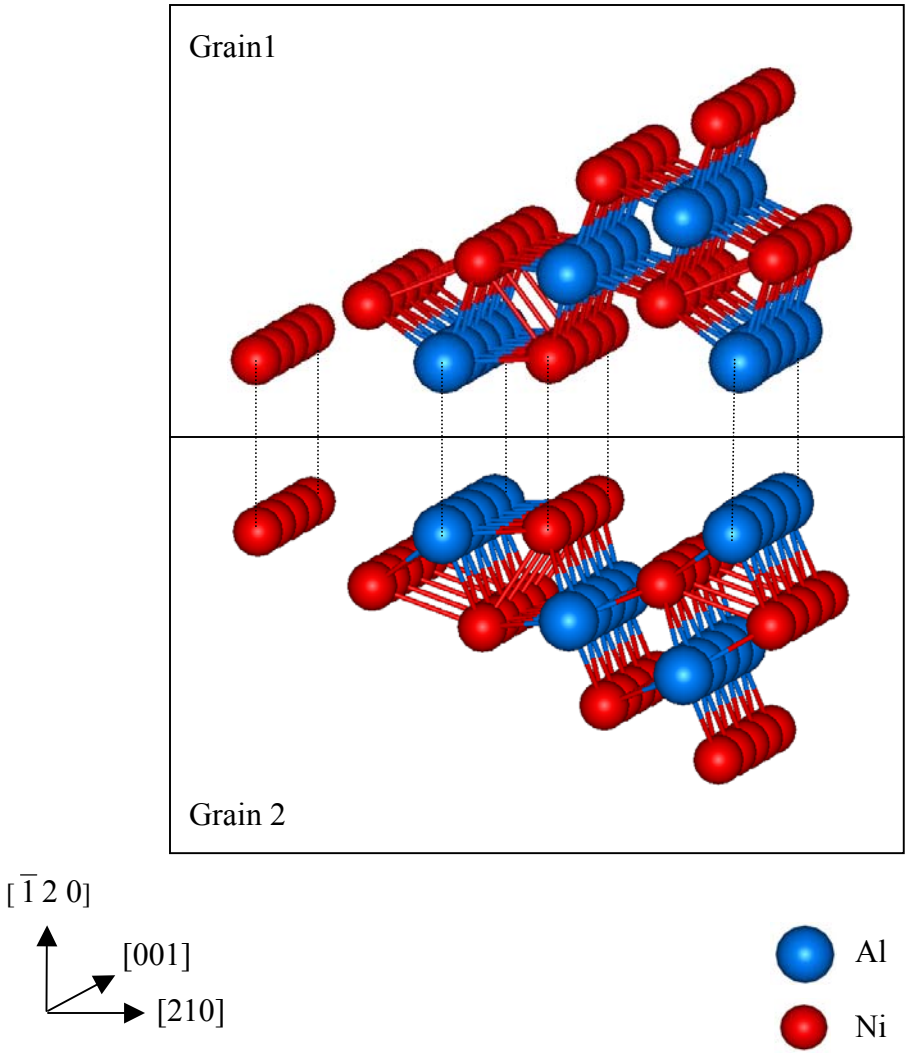

Figure 4.2: Configuration of grains 1 and 2 after a 180° rotation about the [$\bar{1}$ 2 0] direction.

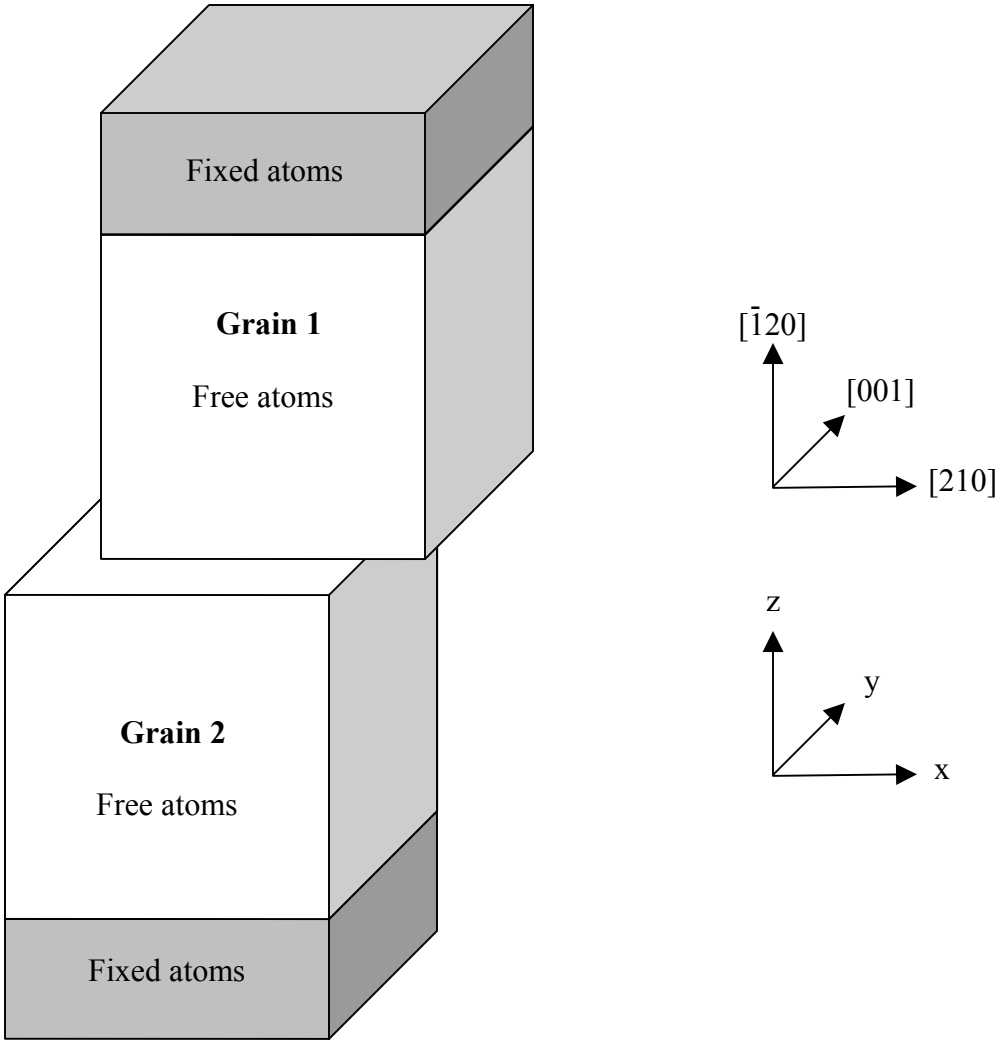

Figure 4.3: Translation of the grain boundary structure.

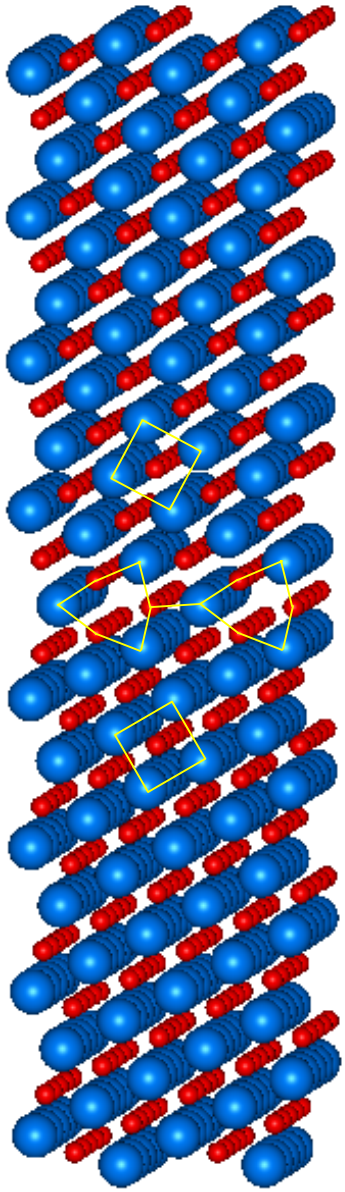

Figure 4.4: Graphical representation of the Σ5(210)[001] grain boundary.

4.2 Molecular Statics Calculation

Molecular statics calculations are performed to determine the relative stability of different configurations of the studied Σ5(210)[001] grain boundary. Three distinct Ni vacancies, whose diffusion is investigated in the MD simulations, are introduced into the GB core. The energy of the resulting structures is then calculated and compared to the energy of the same GB with a Ni vacancy located in the bulk region. The results are reported as the difference in energy between the structure with a vacancy within the GB core and the structure with a vacancy within the GB bulk. Sites 1, 2, and 3, illustrated in figure 4.5, represent the distinct sites where a Ni vacancy is initially introduced. Figure 4.5 also illustrates different sites mentioned later in the investigation. Using the same method, we also calculate the energies of three specific configurations of the grain boundary. These configurations are derived from the MD simulations (see section 4.3.2). Figures 4.6(a), 4.6(b), and 4.6(c) illustrate these three specific configurations. The MS technique is applied to the GB structure constructed above with the same EAM potentials [42] as those used in the bulk investigation.

Table 4.1 shows the calculated energies for the three Ni vacancy sites and the two specific configurations. As expected we obtain different energy values for the different vacancy sites 1, 2, and 3. The configuration with a vacancy in site 1 appears to be the most favorable of the three configurations with an energy value E_{s1}=-0.17 eV. In contrast, the configuration with a vacancy in site 3 is seen to be the least favorable with a positive energy value E_{s3}=0.10 eV. Table 4.2 shows the energies of the three specific configurations also investigated, which correspond to the extrema values found with E_{c1}=-0.39 eV, E_{c2}=0.21 eV, and E_{c3}=0.54 eV. All three arrangements present a divacancy in sites $2\,\widetilde{2}$ and an Al interstitial between, and the configuration of sites $13'5\,\widetilde{5}$, which differs in the three cases, is seen to have a significant influence on the energy.

Table 4.1: Configuration energy of a Ni vacancy in various GB sites.

	Site 1	Site 2	Site 3
Configuration Energy (eV)	-0.17	-0.11	0.10

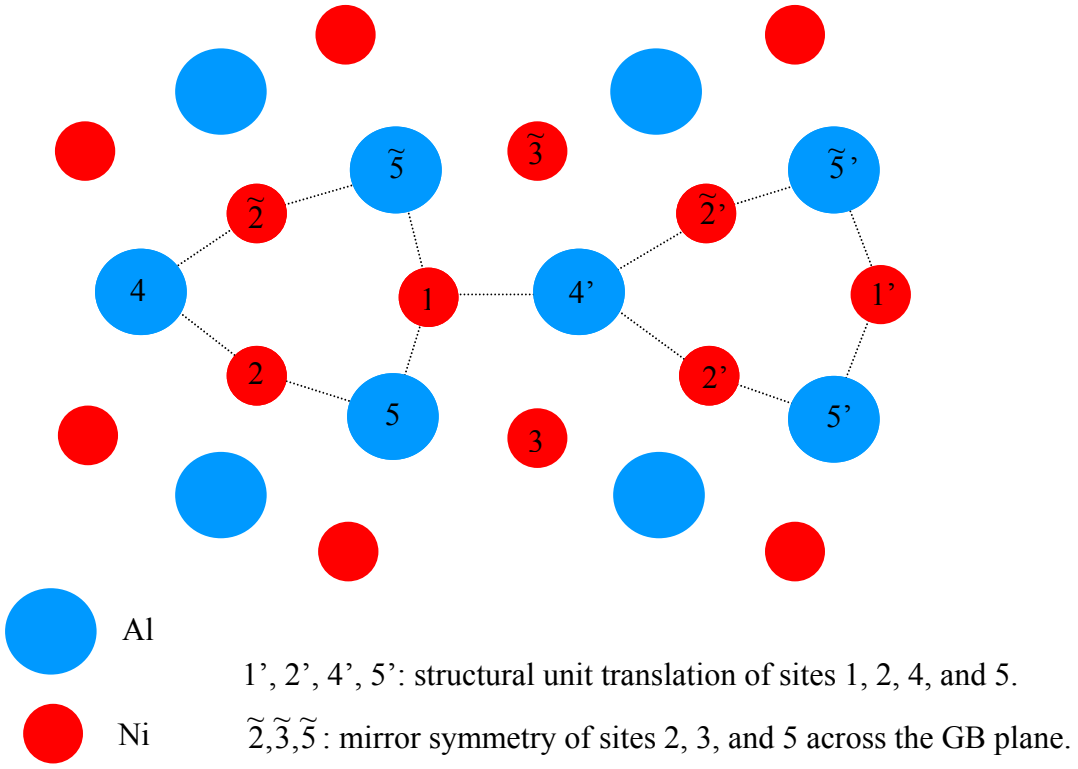

Figure 4.5: Graphical representation of the various vacancy sites.

Table 4.2: Energy of the three specific configurations.

	Configuration 1	Configuration 2	Configuration 3
Energy (eV)	-0.39	0.21	0.54

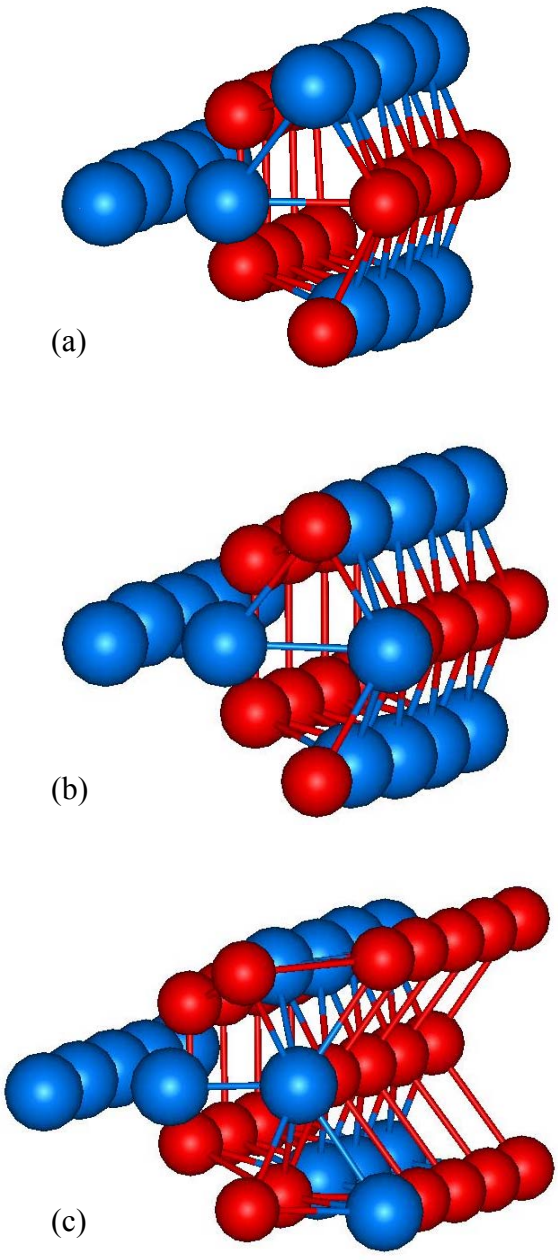

Figure 4.6: Graphical representation of the three specific configurations.

4.3 Molecular Dynamics Investigation

4.3.1 Computational Procedure

The investigation of the grain boundary diffusion is performed with a molecular dynamics simulations code using a constant temperature algorithm, similarly to the bulk diffusion investigation.

A grain boundary Σ5(210)[110] constructed with the technique described in the previous section 4.1 is used. Figure 4.7 illustrates the simulated block used for the present MD investigation. Repeating periodic boundary conditions are applied along the x and y directions, parallel to the grain boundary plane (see fig. 4.5). Fixed boundary conditions are applied in the z direction, normal to the grain boundary plane. The two slabs located at the upper part of grain 1 and the lower part of grain 2 (see gray atoms in fig. 4.5) correspond to fixed atoms whose displacements in the three dimensions remain equal to zero throughout the simulations. The crystal structures within these slabs are perfectly ordered and no geometrical distortions due to the grain boundary core are observed. The thickness of each slab is made larger than the cutoff radius in order to preserve the atomic interactions between free and fixed atoms. The free atoms, which are fully constrained to the equation of motion, are sandwiched between the two slabs of fixed atoms. The grain boundary core is located in the center of the free atom region.

The 460 atoms within the free atom region and the 330 atoms within the two slabs of fixed atoms are arranged in the simulated block with dimensions: 5/3×a[210] in the x direction, 8×a[$\bar{1}$20] in the y direction, and 5×a[001] in the z direction (see fig. 4.5). A Ni vacancy is initially introduced in the sites 1, 1', 2, 2', 5 and 5' in the core grain boundary (see figure 4.5). Sites 1-1', as well as 2-2' and 5-5' are equivalent and correspond to a structural unit translation in the x direction.

The same EAM potentials [42] as in the bulk diffusion study are used to simulate the atomic interactions.

The simulations are performed at different temperatures depending on the site in which the vacancy is initially introduced. Once again, preliminary runs are performed to determine a given temperature for each site that is low enough to keep a high degree of order but high enough to allow the observation of meaningful diffusion phenomena in a

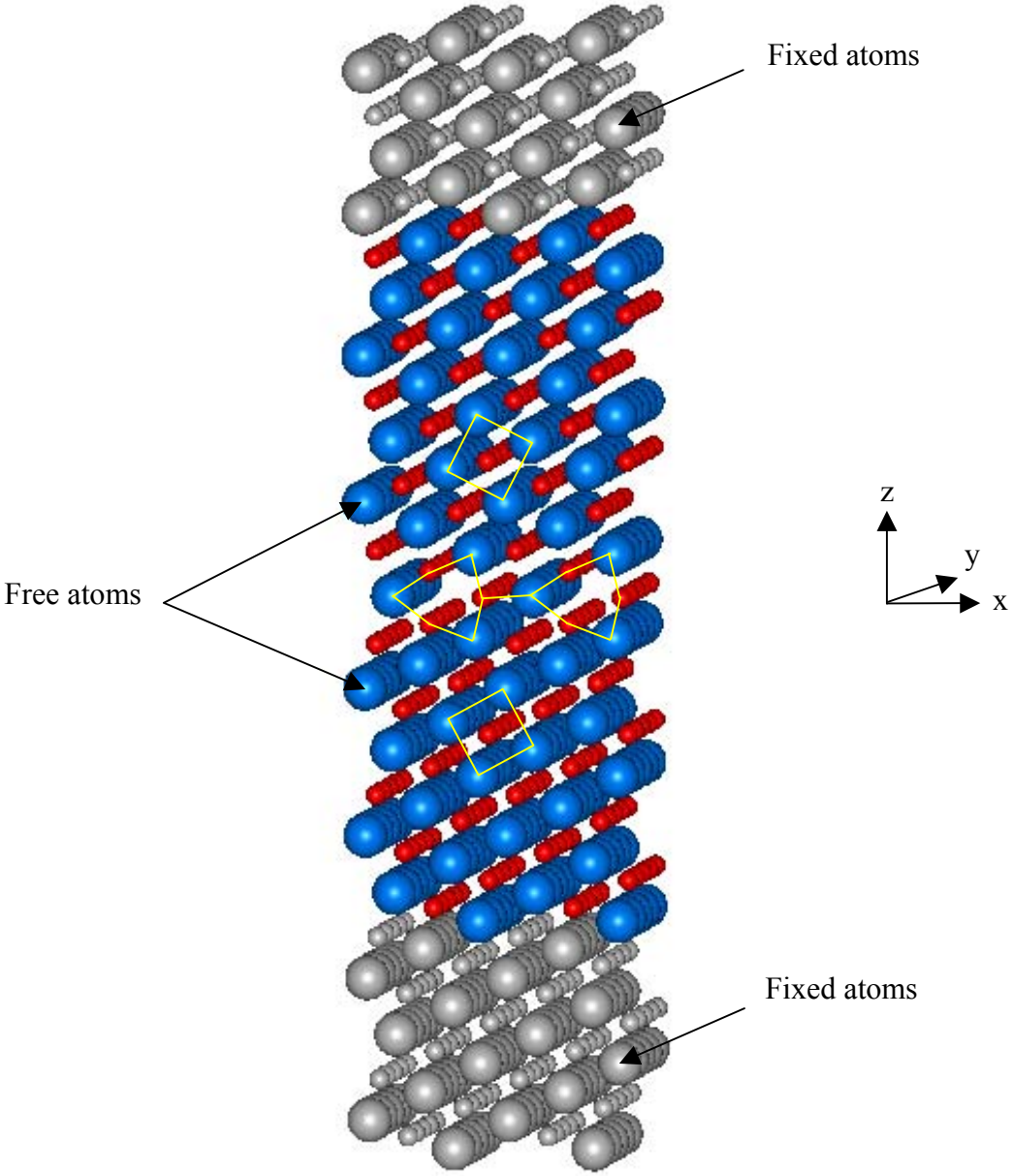

Figure 4.7: Graphical representation of the simulated block.

reasonable computing time. For sites 1 and 1', simulations are performed at both 800 K (527 °C) and 850 K (577 °C). For sites 2 and 2', they are performed at 600 K (327 °C) and 650 K (377 °C), and finally at 550 K (277 °C) and 600 K (327 °C) for sites 5 and 5'.

The diffusion processes are studied over a range of 1,000,000 iterations for all the different sites and at each temperature. With a time step of $4x10^{-6}$ ns, the diffusion phenomena are investigated during 4 ns.

In order to identify and characterize the different mechanisms involved in the grain boundary diffusion, the displacements of the atoms are monitored every 10,000 steps (0.04 ns).

4.3.2 Direct Molecular Dynamics Observations

About 450 jumps are observed in the overall GB investigation. In all the cases where diffusion occurs, the vacancy is seen to migrate via different sequences of coordinated jumps. These jumps are all of a nearest neighbor type except for a specific mechanism, reported below, including one next nearest neighbor jump within the sequence. Depending on the sites in which the vacancy is initially introduced, different types of mechanisms are observed. Most of these mechanisms take place within a single structural unit. They do not contribute to the diffusion along the grain boundary. They yield to a different grain boundary structure that is expected to be competitive with the initial configuration. For the analysis of the results we classify and analyze the different types of diffusion mechanisms as a function of the initial vacancy site.

The grain boundary with an initial vacancy in site 1 exhibits the most stable configuration. The temperatures at which the runs are performed are considerably higher, about 200 K, than for the other initial configurations. This is consistent with the MS calculations reported in section 4.2, where the energy calculated for site 1 is seen to be lower than those of the two other vacancy sites studied.

Two main types of mechanisms are identified for this configuration. The first type corresponds to a vacancy ring mechanism occurring within a single structural unit. The vacancy migrates along a definite path of nearest neighbor jumps leaving a partially

ordered structure behind. The second type of mechanism observed corresponds to the diffusion along the grain boundary. Two distinct sequences of coordinated jumps that result in the vacancy migrating to a neighboring structural unit are identified. In both cases, the vacancy first migrates within a given structure unit as in a ring mechanism, and then, depending on the type of mechanism, reaches a neighboring unit via two coordinated NN jumps or via one direct NNN jumps. As in the vacancy ring mechanism, the order of the structure is not recovered when the sequence is completed and some antisites are left in the path of the vacancy.

The configuration with the initial vacancy in site 2 appears to be less favorable than the previous configuration as seen by the temperatures of 600 K and 650 K at which MD simulations are performed. This is consistent with MS energy calculations as discussed in the previous paragraph.

The MD simulations performed on this GB configuration only highlight one type of sequence where the vacancy migrates within a single structural unit via the ring mechanism mentioned above. No diffusion along the grain boundary is identified.

The third initial configuration, with a vacancy in site 3, is seen to be the least stable of the three configurations. According to the results of the MS calculations that describe this structure as the highest energy configuration, a lower temperature at which the structure starts to evolve is observed in the MD simulations.

Similarly to the previous configuration, only one given type of NN jump sequence is observed. The vacancy first migrates to site 2, and then follows the same ring mechanism as in the configuration of a vacancy in site 2.

4.4 Grain Boundary Diffusion Mechanisms

Two different types of diffusion mechanism arise from the MD investigation reported above. The coming two sections describe these mechanisms on the basis of the direct observations and the configuration energy calculated by MS.

4.4.1 Vacancy Ring Mechanism

The vacancy ring mechanism corresponds to a sequence of coordinated jumps that take place within a single structural unit. The vacancy migrates via nearest neighbor jumps through the different sites 1 2 $\widetilde{2}$ 5 $\widetilde{5}$ of a given unit (see fig. 4.5). The transition between sites 2 and $\widetilde{2}$ is not direct and occurs via an interstitial. The sequence of the vacancy site is obviously determined by the initial configuration. Specific antisites corresponding to jumping atoms that only perform one NN jump are left in the vacancy path, and the structure resulting from this mechanism is partially ordered. The point defect configuration corresponding to a divacancy in 2-$\widetilde{2}$ and an Al interstitial located between these two sites is always observed. However, the final configuration of the structure is dependent on the site into which the vacancy is initially introduced because the final configuration of sites 1 5 $\widetilde{5}$ differs.

As reported in section 4.3.2 this mechanism is observed in the three vacancy site configurations. It is the most common diffusion mechanism observed.

The vacancy ring mechanism observed with a starting vacancy in site 1 is illustrated in figure 4.8. The vacancy migrates along a definite path of nine jumps and the final configuration of the GB structure is a divacancy in sites 2 - $\widetilde{2}$, an Al interstitial, and a Ni atom in site 5 (see fig. 4.6(a)). On the basis of the energy calculations done in section 4.2, this final configuration (reported as configuration 1 in section 4.2), with an energy E_{c1}=-0.17 eV, is seen to be slightly more favorable than the initial configuration with E_{s1}=-0.11 eV. It is then consistent that the system tends to evolve towards this structure through a vacancy ring mechanism.

The sequence related to the vacancy ring mechanism with an initial vacancy in site 2 (see fig. 4.9) is completed in seven atomic jumps. The final configuration presents a lower degree of order than the previous case with an identical configuration for sites 2 - $\widetilde{2}$, but three antisites in 1, 5, and $\widetilde{5}$ (see fig. 4.6(b)). From the MS calculations, this resulting configuration (see configuration 2 in section 4.2) is seen to have a much higher

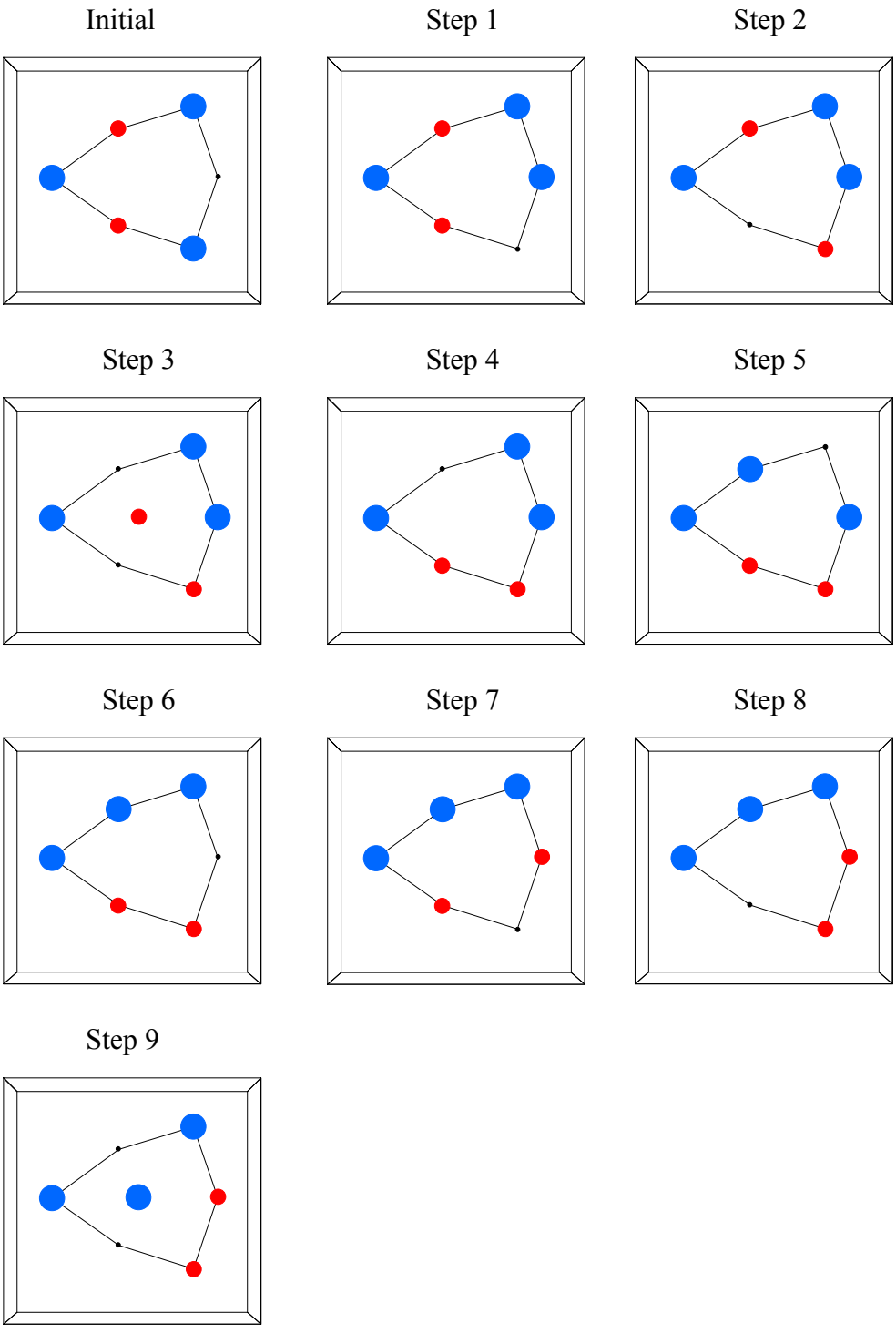

Figure 4.8: Graphical representation of a vacancy ring mechanism with a starting vacancy in site 1.

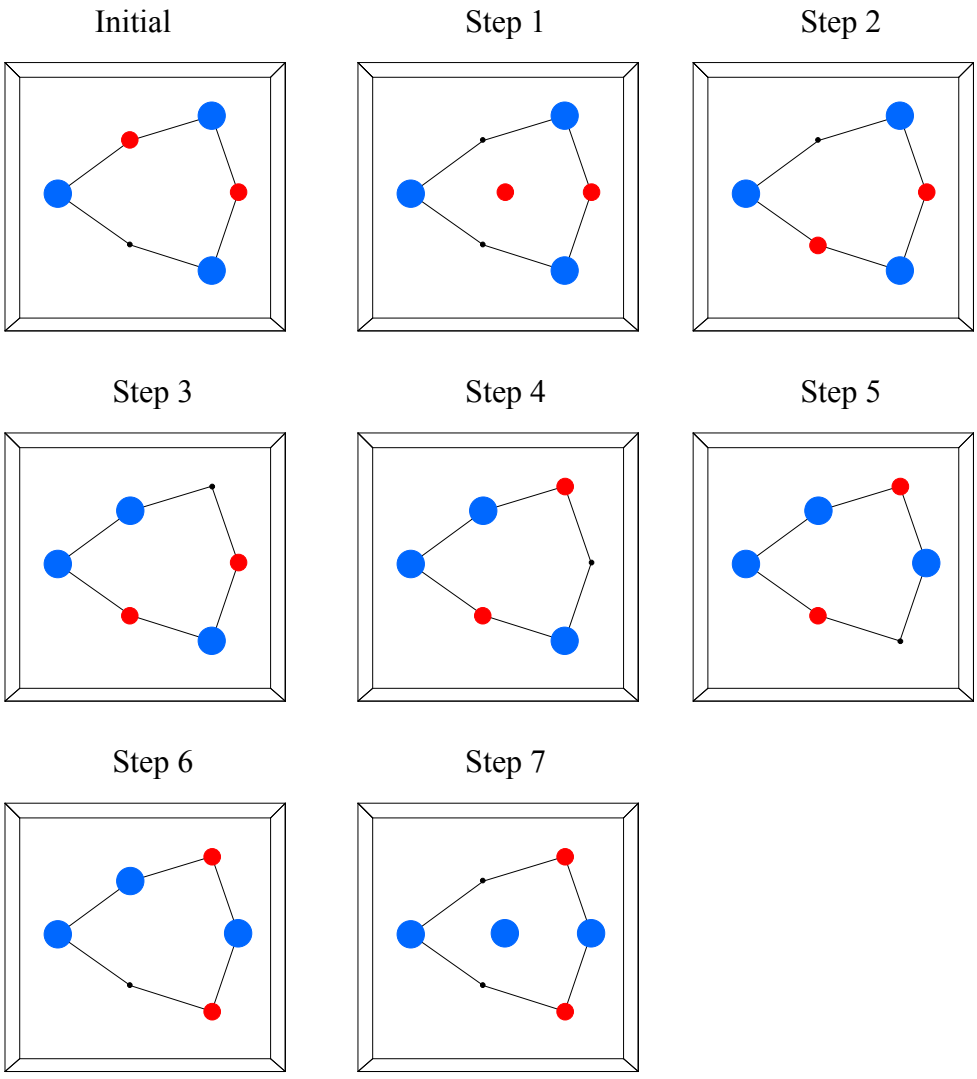

Figure 4.9: Graphical representation of a vacancy ring mechanism with a starting vacancy in site 2.

energy than the previous configuration 1. The two extra antisites result in an energy increase of $\Delta E=E_{c2}-E_{c1}=0.6$ eV. This configuration also appears to be less favorable than the initial configuration with a vacancy in site 2.

The vacancy ring mechanism observed for the last type of initial configuration is identical to the ring mechanism observed for the configuration with a vacancy in site 2. However the final configuration is different because of the presence of two extra antisites in 3 and 5 (see fig. 4.6(c)), created when the vacancy initially migrates to site 5 then to site 2 via NN jumps. The energy of this configuration is, as expected, higher than that of the previous configuration. The MS calculations report an extra energy of $\Delta E=E_{c3}-E_{c2}=0.33$ eV for configuration 3 relative to the configuration 2. Similarly to the previous case, the configuration resulting from this sequence has a considerably higher energy than the initial configuration.

4.4.2 Long Jump Vacancy Diffusion Mechanisms

The mechanisms reported in this section characterize the diffusion along the grain boundary structure where the vacancy is seen to migrate to a neighboring structural unit. These are important for actual matter transport along the GB and they would have a significant contribution to the diffusion coefficient. Two distinct mechanisms are identified in this GB investigation, and they both occur with an initial vacancy in site 1. These long jump vacancy diffusion mechanisms appear to occur with a very low probability and only one of each type of mechanism is observed in the overall GB investigation. Figure 4.10 and 4.11 illustrate the two observed mechanisms where the vacancy migration takes place along the x and -x direction respectively.

For both mechanisms, the vacancy is seen to first perform a series of four coordinated nearest neighbor jumps within the unit before migrating to the neighboring unit as in a vacancy ring (see steps 1 to 5 in fig. 4.10 and 1 to 4 in fig. 4.11). The transition between sites 2 and $\widetilde{2}$ also occurs via an interstitial. The next step, corresponding to the vacancy migration between structural units is different for the two

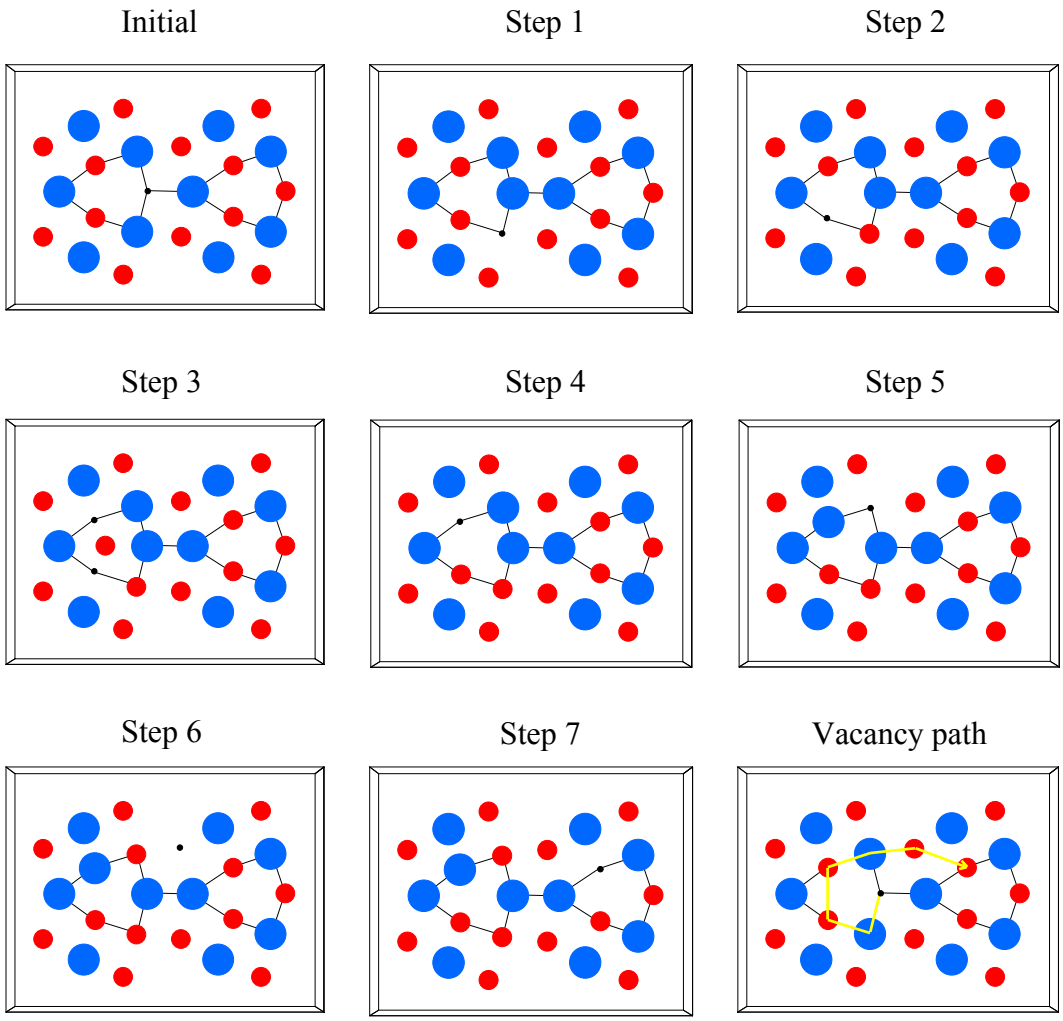

Figure 4.10: Graphical representation of the first type of long jump vacancy diffusion mechanism.

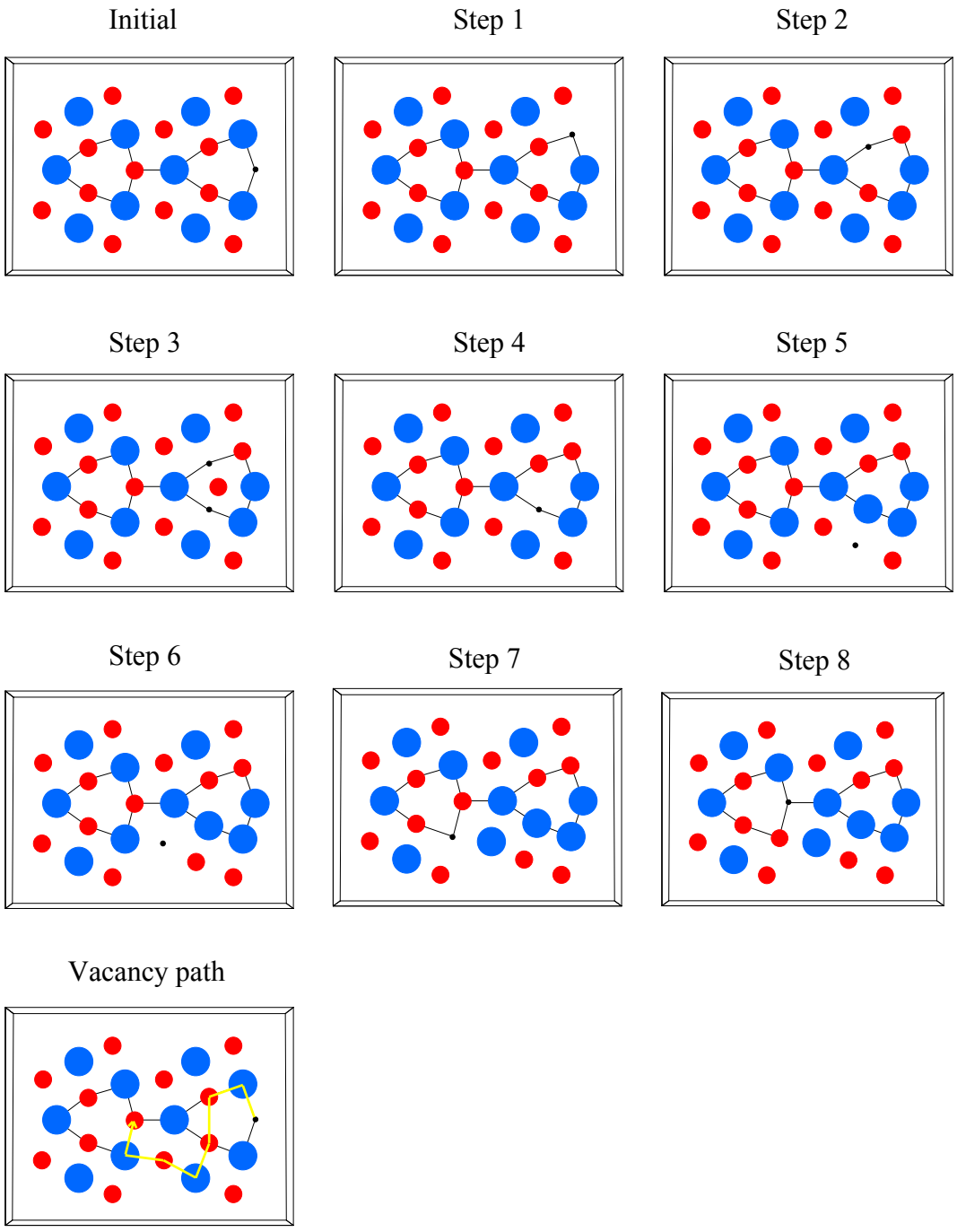

Figure 4.11: Graphical representation of the second type of long jump vacancy diffusion mechanism.

mechanisms. Whereas the vacancy migration between sites $\widetilde{3}$ and $\widetilde{2}$' is direct and occurs via a NNN jump for the first type of mechanism (see step 6 in fig. 4.10), the corresponding migration occurs through the transition 2' 6 3, via two NN jumps, for the second type of mechanism (see step 5, 6 in fig. 4.11). In the two mechanisms, most of the sequence takes place via consecutive NN jumps that introduce disorder. Contrary to cyclic mechanisms, such as 6JPCs or 10JPCs, the vacancy does not migrate through given sites twice recovering the order of the structure.

The transition $\widetilde{3}$ $\widetilde{2}$' observed in the first type of mechanism has also been reported by Sørensen et al. [30] in an investigation of a Σ5(310)[100] Cu grain boundary. However, the comparison can only be done to some extent because of the difference in crystal structure (FCC for Cu and B2 for NiAl). Moreover the migration between sites 1 and $\widetilde{2}$' is seen to occur via two coordinated NNN jumps as illustrated in figure 1.11 for the Cu GB, and not through a complex sequence reported in figure 4.10.

Even if these two mechanisms have only been observed with a starting vacancy in site 1, they are expected to occur with the two other types of initial configurations studied as well. Considering that these mechanisms occur with a very low probability, the fact they are not observed for the other vacancy sites may be due to a probability issue.

Chapter 5
DISCUSSION AND CONCLUSIONS

In the present work, we investigate the vacancy assisted diffusion mechanisms in a perfectly ordered NiAl B2 compound. The diffusion in the bulk as well as at the grain boundary is studied following the same approach. The two simulation techniques, Molecular Statics and Molecular Dynamics, are combined to identify and study the contribution of the different mechanisms involved in the overall diffusion process. The same EAM potentials [42] developed to fit NiAl properties are used in the investigation.

The activation energies of the two diffusion mechanisms expected to take place in the bulk are determined by MS calculations. The value calculated for a Ni vacancy NNN mechanism, is found to be consistent with experimental data [46, 47], and slightly lower than that of the corresponding Al vacancy mechanism. The activation energies calculated for the 6JPCs are seen to be close for both type of vacancy mechanisms, and considerably lower than those of the NNN mechanism. It is important to point out that all of the temperature entropy effects that become important at high temperature are neglected by using MS. Therefore, these results are only relevant at a 0 K temperature. However, the difference in energy between the two mechanisms is so significant, 0.73 eV for Ni and 0.86 eV for Al, that it is reasonable to consider the 6-jump cycle as more favorable than a NNN mechanism, even at high temperature.

The direct observation of the diffusion in the bulk is done through the molecular dynamics investigation. For both point defects, a Ni and Al vacancy, the 6JPC is seen to be the main diffusion mechanism. In agreement with the activation energy calculations, no next nearest neighbor jumps are identified. The detailed analysis of the 6JPC reveals that the [110] type is the most common mechanism. This result is in contrast with *ab*

initio calculations [9,10], but agrees with experimental results [12,13,14] suggesting that Fe mainly diffuses via [110] 6JPCs in B2 FeAl. Other types of events such as the failed cycle attempts are also identified in the MD simulations. The nature of these attempts and the probability with which they occur are seen to be consistent with the migration energy curves determined by MS.

Detailed sequential analyses of [110] 6JPCs are done by focusing the MD simulations. Displacement vs. time curves are determined for both Ni and Al vacancy mechanisms. The profiles of these curves suggest that given jumps are correlated within the sequence. The system is seen to avoid the high-activated states reported by the migration energy curves. This direct observation of correlated jumps in NiAl has also been suggested in B2 FeAl [9, 48] as being a way for the system to avoid high-energy intermediate states.

Two new cyclic mechanisms: the 10 and 14-jump cycles are identified through this bulk diffusion investigation. Whereas the 14-jump cycle is a rare event that is only observed for a Ni vacancy at 1150 K, the 10-jump cycle is seen to contribute to the overall diffusion and cannot be neglected. These two mechanisms describe sequences that are geometrically very similar to those of the different 6JPCs. The analysis of the intermediate point defect configuration reveals that the 6, 10, and 14-jump cycles show that the configurations introducing the largest local distortion is identical in all three cases. The highest activated state, corresponding to this configuration for the 6JPC, may be expected to be identical for the two new cyclic mechanisms. The significant difference in diffusivity observed between the cyclic mechanisms may then be expected to come from correlation effects.

We can also point out that this investigation is performed on a perfectly ordered B2 compound of stoichiometric composition. It is then consistent that no other mechanism, such as the triple defect, the A6JPC, or the ASB, requiring a non-stoichiometric and partially ordered structure is observed.

The stability of Σ5(210)[100] tilt GB structures with specific Ni vacancies within the GB core is investigated via MS calculations. The energy of these configurations is compared to the energy of the same GB with a vacancy located in the bulk region. As

expected, the energies found vary from site to site. They are lower than in the lattice for sites 1 and 2 belonging to the structural unit, and higher for site 3 located outside the unit.

MD simulations are performed at various temperatures for the three initial configurations whose configuration energy is calculated by MS. The temperatures of investigation are seen to vary accordingly to the configuration energies. Thus, the diffusion appears to take place at the lowest temperature for the highest energy configuration, e.g. for site 3, and at the highest temperature for the lowest energy configuration, e.g. for site 1.

Two different types of GB mechanisms are highlighted by the MD investigation: the vacancy ring mechanism and the long jump vacancy mechanisms. These two types of mechanisms yield to a partially ordered structure that is not recovered when the mechanisms are completed.

The vacancy ring mechanism corresponds to a sequence of coordinated NN jumps taking place within a structural unit. The configuration resulting from this mechanism is seen to be energetically favorable when it takes place with a starting vacancy in site 1 and significantly unfavorable for the two other initial configurations.

The long jump vacancy mechanisms characterize the diffusion along the grain boundary, where the vacancy is seen to migrate to a neighboring structural unit. Two distinct mechanisms are identified where the transition between neighboring structural units occurs via one direct NNN jump, or via two coordinated NN jumps. We can point out that the specific transition occurring via NNN jump described above corresponds to the only NNN jump observed in the entire investigation.

The use of the molecular Dynamics was motivated by the ability of the technique to reproduce the physical behavior of the system by including intrinsically the entropy and correlation effects. Thus, the diffusion mechanisms taking place in the system could be identified by direct observation without any *a priori* assumption. Once again, it is important to stress that the accuracy of this technique, as well as the MS technique, is strongly dependent on the potentials used.

Appendix A

Generic MD input file used in the bulk investigation

assign dimensions of the simulated block

box 14.6845 14.6845 14.6845

define lattice

read lattice_1200.par

define periodic boundary condition in x y z

surface off x y z

define interatomic potentials

read nialf.pot

define type and mass of atoms

typename 1 Ni 2 Al

select type 1

mass 58.71

select type 2

mass 26.982

select all

define time step

dtime 2.E-15

define initial position of the atom

refstep

assign initial temperature

itemp 1200

assign temperature at which MD is performed

clamp 1200

assign number of MD steps

cmd 50000

define a loop

repeat 24

assign number of MD steps within a loop

cmd 50000

calculate displacements of each atom

disp refcalc

select all

write displacements of each atom within a file

write FILE +disp_ni_1200_50-1250.disp sel disp

write energies of each atom within a file

write FILE +en_ni_1200_50-1250.eatom sel EATOM

end of the loop

end

assign number of quench steps

quench 1000

calculate displacements of each atom

disp refcalc

select all

write displacements of each atom within a file

write FILE disp_ni_1200_1250_q.disp sel disp

REFERENCES

[1] A. T. Donaldson and R. D. Rawlings, Acta Metallurgica, **24**, 285 (1976).

[2] A. Lutze-Birk and H. Jacobi, Scripta Metallurgica, **9**,761 (1975).

[3] H. Hahn, G. Frohberg, and H. Wever, Physic State Solid (a), **79**, 559 (1983).

[4] Y. Mishin and D. Farkas, Philosophical Magazine A, **75**, 187 (1997).

[5] E. W. Elcock and C. W. McCombie, Physical Review,**109**, 6 (1958).

[6] P. Wynblatt, Acta Metallurgica, **15**, 1453 (1967).

[7] I. V. Belova, M. E. Ivory, and G. E. Murch, Philosophical Magazine A, **72**, 87 (1995).

[8] C. R. Kao, K. Sungtae, and Y. A. Chang, Materials Science and Engineering A, **192/193**, 965 (1995).

[9] R. Drautz and M. Fähnle, Acta Metallurgica et Materiala, **47**, 2437 (1999).

[10] M. Arita, M. Kiowa, and S. Ishioka, Acta Metallurgica et Materiala, **37**, 1363 (1989).

[11] S. Ishioka and M. Kiowa, Philosophical Magazine A, **52**, 267 (1985).

[12] G. Vogl and B. Sepiol, Acta Metallurgica et Materiala, **42**, 3175 (1994).

[13] B. Sepiol, C. Czihak, A. Meyer, G. Vogl, J. Metge, and R. Rüffer, Hyperfine Intereaction, **113**, 449 (1998).

[14] R. Weinkamer, P. Fratzl, B. Sepiol, and G. Vogl, Physical Review B, **59**, 8622 (1999).

[15] M. Kaisermayr, J. Combet, H. Ipser, H. Schicketanz, B. Sepiol, and G. Vogl, Physical Review B, **61**, 12038 (2000).

[16] N. A. Stolwijk, M. van Gend, and H. Bakker, Philosophical Magazine A, **42**, 783 (1980).

[17] M. Athènes, P. Bellon, and G. Martin, Philosophical Magazine A, **76**, 565 (1997).

[18] C. R. Kao and Y. A. Chang, Intermetallics, **1**, 237 (1993).

[19] R. W. Fonda, M. Yan, and D. E. Luzzi, Philosophical Magazine Letters, **71**, 221 (1998).

[20] Y. Mishin and D. Farkas, Philosophical Magazine A, **78**, 29 (1998).

[21] R. E. Hoffman, Acta Metallurgica, **4**, 56 (1956).

[22] J. Sommer, Chr. Herzig, S. Meyer, and W. Gust, Defect and Diffusion Forum, **6669**, 843 (1989).

[23] D. Turnbull and R. E. Hoffman, Acta Metallurgica, **2**, 419 (1954).

[24] Q. Ma and R. W. Balluffi, Acta Metallurgica et Materiala, **41**,133 (1993).

[25] E. Budke, Chr. Herzig, S. Prokofjev, and L. S. Shindlerman, Materials Science Forum, **207-209**, 465 (1996).

[26] Y. Mishin, Philosophical Magazine A, **72**, 1589 (1995).

[27] T. Kwok, P. S. Ho, S. Yip, R. W. Baluffi, P. D. Bristowe, and A. Brokman, Physical Review Letters,**47**,1148 (1981).

[28] C. L. Liu and S. J. Plimpton, Physical Review B, **51**, 4523 (1995).

[29] M. Nomura and J. B. Adams, Journal of Materials Research, **10**, 2916 (1995).

[30] M. R. Sørensen, Y. Mishin, and A. F. Voter, Physical Review B, **62**, 3658 (2000).

[31] N. Metropolis, A. W. Rosenbluth, M. N. Rosenbluth, A. H. Teller, and E. Teller, Journal of Chemistry Physics, **21**, 1087 (1953).

[32] B. J. Alder and T. E. Wainwright, Journal of Chemisrty Physics, **27**, 1208 (1957).

[33] W. G. Hoover, Lecture Note in Physics: Molecular Dynamics, edited by H. Arita, Kyoto, J. Ehlers, München, K. Hepp, Zürich, R. Kippenhahn, München, H. A. Weidenmüller, Heidelberg, and J. Zittartz, Köln, page13, Springer-Verlag, 1986.

[34] J. M. Haile, Molecular Dynamics Simulation Elementary Methods, page 40-42, Wiley-Interscience (1992).

[35] J. Rifkin, XMD, http://www.ims.uconn.edu/centers/simul/index.htm#xmd.

[36] J. Tersoff, Physical Review B, **39**, 5566 (1989).

[37] F. H. Stillinger and T. A. Weber, Physical Review B, **31**, 5262 (1985).

[38] J. E. Sinclair and R. Fetcher, Journal of Physics C, **7**,864 (1972).

[39] H. Hohenberg and W. Kohn, Physical Review, **136**, 13864 (1964).

[40] J. Rose, J. Smith, and J. Ferrante, Physical Review B, **28**, 1835 (1983).

[41] R. Pasianot, D. Farkas, and E. Savino, Physical Review B, **43**, 6952 (1991).

[42] D. Farkas, B. Mutasa, C. Vailhé, and K. Ternes, Modeling and Simulation in Materials Science and Engineerning, **3**, 210 (1995).

[43] A. F. Voter and S. P. Chen, Materials Research Society Symposium Proceedings, **82**, 175 (1987).

[44] A. I. Rao, C. Woodward, and T. A. Parthasarathy, Materials Research Society Symposium Proceedings, **213**, 125 (1991).

[45] Y. Mishin and D. Farkas, Philosophical Magazine A, **75**, 169 (1997).

[46] G. F. Hancock and B. R. McDonnel, Physica Status Solidi A, **4**, 143 (1971).

[47] S. Divinski and Chr. Herzig, Intermetallics, **8**, 1357 (2000).

[48] J. Mayer and M. Fähnle, Defect Diffusion Forum, **143-147**, 285 (1997)

VITA

The Author was born on October 22th, 1977 in Tonneins (France). After completing his high school education, he joined the Université de Technologie de Compiègne (France), where he completed his undergraduate degree in Mechanical Engineering. After a six-month internship at DaimlerChrysler, Stuttgart (Germany), the author enrolled in the Master Program in the department of Materials Science and Engineering at Virginia Tech, Blacksburg (USA). He joined the Center for Modeling and Simulation in Materials Sciences and focused his research on diffusion in B2 compounds. The author now intends to enroll in a PhD Program with the Center for Electronic Structure of Materials at Flinders University, Adelaide (Australia).

Benjamin J. Soulé de Bas